1 **Algal lipids reveal unprecedented warming rates in alpine areas of SW Europe**

2 **during the Industrial Period**

4 Antonio García-Alix[1,2,3*], Jaime L. Toney[2], Gonzalo Jiménez-Moreno[1], Carmen Pérez-

5 Martínez[4], Laura Jiménez[4], Marta Rodrigo-Gámiz[1], R. Scott Anderson[5], Jon Camuera[6],

6 Francisco J. Jiménez-Espejo[3], Dhais Peña-Angulo[7], María J. Ramos-Román[6]

9 [1] Department of Stratigraphy and Paleontology, University of Granada, Granada, 18072,

10 Spain.

11 [2] School of Geographical and Earth Sciences, University of Glasgow, Glasgow, G12

12 8QQ, UK.

13 [3] Instituto Andaluz de Ciencias de la Tierra (IACT), CISC-UGR, Armilla, 18100, Spain.

14 [4] Department of Ecology and Institute of Water Research, University of Granada,

15 Granada, 18072, Spain.

16 [5] School of Earth and Sustainability, Northern Arizona University, Flagstaff, AZ 86011,

17 USA.

18 [6] Department of Geosciences and Geography, University of Helsinki, Helsinki, FI-00014,

19 Finland.

20 [7] Department of Geography, University of Zaragoza, Zaragoza, 50009 Spain.

22 *Correspondence to:* Antonio García-Alix (agalix@ugr.es)

24 **Abstract.** Alpine ecosystems of the southern Iberian Peninsula are among the most

25 vulnerable and the first to respond to modern climate change in southwestern Europe.

26 While major environmental shifts have occurred over the last ~1500 years in these alpine

27 ecosystems, only changes in the recent centuries have led to abrupt environmental

28 responses, but factors imposing the strongest stress have been unclear until now. To

29 understand these environmental responses, this study, for the first time, has calibrated an

30 algal lipid-derived temperature proxy (based on long-chain alkyl diols) to instrumental

31 historical data extending alpine temperature reconstructions to 1500 years before present.

32 These novel results highlight the enhanced effect of greenhouse gases on alpine

33   temperatures during the last ~200 years and the long-term modulating role of solar
34   forcing. This study also shows that the warming rate during the 20th century
35   (~0.18ºC/decade) was double that of the last stages of the Little Ice Age
36   (~0.09ºC/decade), even exceeding temperature trends of the high-altitude Alps during the
37   20th century. As a consequence, temperature exceeded the pre-industrial records in the
38   1950s, and was one of the major forcings of the enhanced recent change in the alpine
39   ecosystems from southern Iberia. Nevertheless, other factors reducing the snow and ice
40   albedo (e.g., atmospheric deposition) may have influenced local glacier loss, since almost
41   steady climate conditions predominated from middle 19th century to the first decades of
42   the 20th century.

1. Introduction

46   Global mean annual surface temperatures have risen by ~0.85ºC from 1880 to
47   2012 and the recent decades have been the warmest in the Northern Hemisphere during
48   the Common Era (IPCC, 2013). This trend is alarming, since over the last decade
49   temperature records have been broken yearly. For example, in Spain the highest
50   temperatures ever recorded in September and July occurred in 2016 (45.5ºC) and 2017
51   (46.9ºC-47.3ºC), respectively (Spanish National Weather Agency - AEMet Open Data,
52   2019). Increasing global temperatures are contributing not only directly to land and ocean
53   surface warming, but are also changing the global hydrological cycle through the
54   disturbance of atmospheric circulation patterns and moisture (Easterling et al., 2000;
55   IPCC, 2013). As a result, the term "global warming" is migrating towards recent "climate
56   change" in order to express the variety of modern climate extremes witnessed across the
57   world. The effects of modern global warming and associated climate change events may
58   be causing extreme environmental impacts, beyond what is recorded in the recent
59   geologic record (Waters et al., 2016). Hence, it is crucial to identify warming thresholds,
60   rates, and forcing mechanisms from past high-resolution temperature records to
61   understand modern climate change. It is especially important in fragile regions such as
62   high elevation ecosystems of the Mediterranean alpine realm, an environmentally
63   vulnerable biodiversity "Hot-Spot" (Giorgi, 2006; Schröter et al., 2005) where recent
64   climate change is affecting species richness and distribution (Médail and Quézel, 1999;
65   Pauli et al., 2012). Therefore, alpine wetlands in the Mediterranean region, such as the

ones from the Sierra Nevada in the southern Iberian Peninsula, are sensitive recorders of changing climate and their sedimentological records archive the ecological and biogeochemical responses to different environmental forcings (Catalan et al., 2013).

In order to contribute to a better understanding of recent climate change events in these vulnerable areas, here, for the first time, we calibrate a recently developed algal lipid-derived temperature proxy in an alpine lacustrine record that overlaps with instrumental temperature time-series. This calibration allows the reconstruction of temperatures in alpine areas of the southern Iberian Peninsula during the Common Era when instrumental records are discontinuous or non-existent. Temperature-dependent biomarkers, such as those produced by algae (alkenones) or bacteria/archaea (glycerol dialkyl glycerol tetraethers: GDGTs) have been commonly used in a wide range of marine records as quantitative paleothermometers, and their further application in lake environments has widely increased in the last decade (e.g., Castañeda and Schouten, 2011; Colcord et al., 2015; Foster et al., 2016; Longo et al., 2018; Theroux et al., 2010). Another promising type of algal lipid biomarkers, the long-chain alkyl diols (hereafter LCDs), have also been assessed as temperature proxy in marine environments (Rampen et al., 2014b; Rampen et al., 2012; Rodrigo-Gámiz et al., 2014; Rodrigo-Gámiz et al., 2015). Nevertheless, the relationship between LCDs and temperature has only been tentatively tested in freshwater environments (Rampen et al., 2014a). In this regard, studies using LCDs as (paleo)environmental proxies in marine environments (not just only for temperature reconstructions) have increased in the last years, showing the potential of LCDs as proxies for upwelling (Rampen et al., 2008; Versteegh et al., 1997; Willmott et al., 2010), riverine inputs to marine settings (de Bar et al., 2016; Lattaud et al., 2017a; Lattaud et al., 2018a), or nutrient inputs (Gal et al., 2018). Nevertheless, only a few studies have tested LCDs as lacustrine archives of paleoproductivity (Shimokawara et al., 2010), past rainfall anomalies (Romero-Viana et al., 2012), or temperatures (Rampen et al., 2014a), among others. In any case, despite the great potential of LCDs for paleoenvironmental reconstructions, a number of questions exist about the applicability of diols in high latitude areas (Rodrigo-Gámiz et al., 2015), in freshwaters records (Rampen et al., 2014a), and about the distribution and sources of the biological producers (Balzano et al., 2018; Villanueva et al., 2014; Yu et al., 2018).

99   The LCD distribution in marine environments shows significant correlations with

100   mean annual sea surface temperature through the ratio of the fractional abundances of C_{28}

101   1,13-diol, C_{30} 1,13-diol, and C_{30} 1,15-diol that are used in the Long chain Diol Index (LDI,

102   Eq. (1)) (Rampen et al., 2012). The application of LCDs as a temperature proxy is novel

103   in freshwater environments and only two preliminary calibrations based on recent surface

104   sediments have been obtained using both mean annual air temperatures (weather station

105   data) and organic-derived temperature proxies (GDGTs) (Rampen et al., 2014a). Here,

106   we improve the biomarker paleothermometry by establishing the first temperature

107   calibration for freshwater LCDs using a comparison with historical temperature records

108   for the last ~100 years. Although this calibration can only be applied to the studied lake

109   at present, and perhaps to other alpine wetlands in the Sierra Nevada area, these new data

110   support and reinforce the promising use of LCDs as a paleotemperature proxy in

111   freshwater environments.

112

113   Equation (1) LDI= $(F_{C_{30}}$ 1,15-diol$)/(F_{C_{28}}$ 1,13-diol + $F_{C_{30}}$ 1,13-diol + $F_{C_{30}}$ 1,15-diol$)$

114   (Rampen et al., 2012)

115

116   **1.1 Regional settings**

117

118   This paper focuses on the LCD record of two adjacent cores from Laguna de Río

119   Seco (LdRS), a small alpine lake (~0.42 ha and less than 3m of water depth) at 3020 masl

120   in the protected Sierra Nevada National Park, southern Spain (Fig. 1). Alpine Sierra

121   Nevada wetlands, including LdRS, are low primary production (oligo-mesotrophic)

122   systems and their biogeochemical cycles partially depends on aeolian nutrient supplies

123   (e.g., Saharan aerosol deposition), since catchment basins are small and barren in

124   nutrients (Morales-Baquero et al., 2006; Pulido-Villena et al., 2005; Reche et al., 2009).

125

126   Sierra Nevada is the southwestern-most mountain range in Europe, where latest

127   Pleistocene cirque glaciers carved the metamorphic (mica schist) bedrock in the highest

128   peaks (Castillo Martín, 2009). Massive glacier melting at the latest Pleistocene-Holocene

129   transition transformed the former glacial depressions into lacustrine areas (Castillo

130   Martín, 2009) that evolved gradually into either shallow lakes or peatlands around the

131   middle-to-late Holocene transition (Garcia-Alix et al., 2017; Jiménez-Espejo et al., 2014).

132   Small glaciers re-appeared at the highest peaks of the Sierra Nevada in the 15th century,

during the Little Ice Age (LIA), and remained until the 20th century (Oliva et al., 2018). The presence of these glaciers is observed in the sedimentary record of some alpine lakes and wetlands in the Sierra Nevada as deposit of coarse sediments, like Laguna de la Mosca on the north face of the Sierra Nevada (Oliva and Gomez-Ortiz, 2012). However, these kinds of deposits have not been registered in LdRS (south face of the Sierra Nevada), where the last 1500 years are characterised by continuous laminated clays and bryophyte layers (Anderson et al., 2011). Glacial effects have not caused any disturbance on wetland sedimentation (e.g., erosion) and local alpine sedimentary records show continuous sedimentation patterns (Anderson et al., 2011; García-Alix et al., 2012; Jiménez-Moreno and Anderson, 2012; Jiménez-Moreno et al., 2013; Mesa-Fernández et al., 2018; Oliva and Gomez-Ortiz, 2012; Ramos-Román et al., 2016). Conversely, an increase in sedimentation rates have been detected in the last ~200 years, probably resulting from the waning stages of the LIA (Oliva and Gomez-Ortiz, 2012) and enhanced human activities in the alpines areas of Sierra Nevada during the 19th (García Montoro et al., 2016; Titos Martínez, 2019; Titos Martínez and Ramos Lafuente, 2016) and 20th (Jiménez et al., 2015) centuries. These high-sedimentation rates did not affect the natural responses of the local algal communities to environmental variables such as temperature, but there has been a dilution effect of algal compounds (e.g., chlorophylls and labile carotenoids) in the sediments (Jiménez et al., 2015).

During the 20th century this sensitive alpine region of southern Iberia has experienced significant impacts from modern climate change as evidenced, for example, by the first permanent European glacier loss there during the first half of the 20th century (Grunewald and Scheithauer, 2010) and the extreme permafrost reduction during recent decades (Oliva and Gomez-Ortiz, 2012). This melting supplied a large volume of freshwater (Jiménez et al., 2019) that boosted the water availability in the area and the occasional development of local aquatic environments, contrasting with the general environmental aridification trend observed throughout the 20th century (Garcia-Alix et al., 2017; Jiménez et al., 2019; Ramos-Román et al., 2016).

The sedimentary archive of LdRS has been selected for this study in order to 1) improve the freshwater LCD paleothermometry by proposing a new temperature calibration for freshwater LCDs in the alpine wetlands of the Sierra Nevada area, 2) reconstruct temperatures beyond the instrumental record in a site at the leading edge of

167 changing climate, 3) assess the role of different radiative forcing (e.g., solar radiation or
168 greenhouse gas concentrations) on temperature change in alpine wetlands of the
169 southwestern Europe during the Common Era, and 4) understand the responses to recent
170 climate change in this highly sensitive environment.
171
172 **2. Materials and methods**
173
174 **2.1. Sediment sampling**
175
176   Two sediment cores were taken at the deepest part of LdRS, an alpine lake at 3020
177 masl in the Sierra Nevada (southern Iberian Peninsula) (Fig. 1). A long sediment core
178 (150 cm) was retrieved in 2006 (LdRS lgc). A short sediment core of 16 cm was collected
179 in 2008 (LdRS shc) using a slide-hammer gravity corer (Aquatic Research Instruments,
180 Hope, Idaho, USA). Independent age models were performed in each sediment core to
181 avoid potential correlation problems caused by changes in the sedimentation rates
182 between both coring sites (Fig. 1c) and different sampling dates (2006-LdRS lgc and
183 2008-LdRS shc). The age model of LdRS lgc is based on ^{210}Pb and ^{137}Cs in the uppermost
184 part (first 15 cm), and ^{14}C analyses in older sediments (Anderson et al., 2011). The age
185 model of the LdRS shc is based on gamma spectroscopy by measuring the ^{210}Pb, ^{137}Cs,
186 and ^{226}Ra radionuclides in the first ~14 cm, and afterwards the age was extrapolated to
187 the core bottom (16 cm) (Jiménez et al., 2019; Jiménez et al., 2018). Both records show
188 that the sediment accumulation rate for the uppermost 15-16 cm ranges between 0.09 and
189 0.13 cm/yr (Anderson et al., 2011; Jiménez et al., 2018), with lower sedimentation rates
190 below this depth (~0.008 cm/yr) (Anderson et al., 2011). Ages models show that the LdRS
191 shc extends back to ~200 years with a sample resolution ranging from 5 to 7 years (high-
192 resolution) (Jiménez et al., 2019; Jiménez et al., 2018). In the case of the LdRS lgc, the
193 section studied in this paper covers the last ~1500 years with a lower sample resolution.
194 In this case, the sample resolution is around 6-7 years in the first 10 cm, and from 24 to
195 150 years in older samples (Anderson et al., 2011).
196
197 **2.2. Geochemical analyses**
198

199   Thirty-two sediment samples were collected consecutively every 0.5 cm along

200   LdRS shc and twenty-one samples in the first 22 cm of LdRS lgc. The samples were

201   freeze-dried and homogenized. The total lipid content was extracted from the sediment

202   samples using a Thermo Scientific™ Dionex™ ASE™ 350 Accelerated Solvent

203   Extractor system at 100ºC and 7×10^6 Pa using a mixture of dichloromethane (DCM) and

204   methanol (9:1, v:v). Afterwards, the neutral fraction was separated by means of

205   aminopropyl-silica gel chromatography using DCM:isopropanol (1:1, v:v). This neutral

206   fraction was subsequently eluted with hexane, DCM, ethyl acetate:hexane (25:75, v:v),

207   and methanol through a 230-400 mesh/35-70 micron silica-gel chromatographic column,

208   in order to obtain four neutral sub-fractions (N1-N4). Long chain diols were obtained in

209   the third neutral fraction (N3, alcohol fraction), which was derivatised by bis-

210   (trimethylsilyl) trifluoroacetamide (BSTFA) before running the analyses. 30μL of

211   BSTFA and 40μL of pyridine were added to each N3 fraction and heated at 80°C for 2

212   hours. When vials were at room temperature, a volume between 140 μl and 220 μl of

213   DCM was added to each sample. Firstly, the derivatised N3 fractions were analysed with

214   a Gas Chromatography with Flame-Ionization Detector (GC-FID Shimadzu 2010). An

215   external standard of cholesterol was measured every five samples in order to estimate the

216   appropriate concentration for mass spectrometry analyses. The sample at 19.5 cm depth

217   in the long core was discarded because its concentration was below detection limits.

218   Subsequently, the N3 fractions were measured in a Shimadzu QP2010-Plus Mass

219   Spectrometer interfaced with a Shimadzu 2010 GC using a scan mode between m/z 50 –

220   650, in order to obtain a general picture of the mass spectrum of the samples and the

221   specific retention times where the C_{28}, C_{30}, and C_{32} diols eluted. Afterwards, samples

222   were re-analysed on the basis of a Selected-Ion Monitoring mode (SIM), selecting the

223   characteristic fragment ions of the most important long chain diols, i.e., m/z 299, 313,

224   327, and 341 (Rampen et al., 2012; Versteegh et al., 1997) and the specific retention time

225   window to identify the C_{28}, C_{30}, and C_{32} diols with the mid-chain alcohol positioned at

226   carbon 13, 14 or 15. Fractional abundances of the C_{28} 1,13-diol, C_{30} 1,13-diol, C_{30} 1,15-

227   diol were used in Eq. (1) to calculate the Long chain Diol Index (LDI) (Rampen et al.,

228   2012). Fractional abundances of C_{28} 1,13-diol, C_{30} 1,13-diol, C_{30} 1,15-diol and C_{32} 1,15-

229   diol were used to characterise the potential diol source (e.g., marine, lacustrine, or specific

230   algae groups) (Lattaud et al., 2018a; Rampen et al., 2014a). Fractional abundances of the

231   C_{28} and C_{30} 1,14-diols were measured only in the short core in order to assess their

232   potential relationship with temperatures (Rampen et al., 2014b). The presence of the $C_{32:1}$

233 1,15-diol has also been tested, but it was only identified in some samples from the short
234 core at very low concentrations, thus is not included it in this study.

235

236 **2.3. Reference temperature time-series for LCD temperature calibrations**

237

238   Generating an accurate temperature calibration based on LCDs in alpine wetlands
239 from the Sierra Nevada area is challenging, because there is a lack of long and continuous
240 temperature time-series at such high elevations. The meteorological observatories at the
241 Sierra Nevada ski resort (ranging in elevation from 2500 to 3020 masl) only provided
242 discontinuous temperature records from 1965 to 2011 (Observatorio del cambio global
243 de Sierra Nevada, 2016; Spanish National Weather Agency - AEMet Open Data, 2019)
244 that show a significant correlation (r>0.95; p<0.0001) with low elevation temperature
245 time-series (Table S1, S2). Therefore, a potential way to obtain a LCD-based temperature
246 calibration is by means of the correlation of LCD data with long and reliable historical
247 temperature time-series at nearby lower elevation areas, followed by a correction for the
248 altitudinal effect on temperatures.

249

250   The three weather observatories in the Granada area, at the foothills of the Sierra
251 Nevada, only provide reliable temperature data from the 1970s onwards (Spanish
252 National Weather Agency - AEMet Open Data, 2019), which is a short-period for an
253 accurate down-core proxy calibration. Temperature time-series preceding the 1970s have
254 been reconstructed using statistical models (e.g., Gonzalez-Hidalgo et al., 2015), and
255 show a good correlation with the LDI and the relative abundance of the C_{28} 1,13-, C_{30}
256 1,13-, and C_{32} 1,15-diols, but a weaker correlation with the C_{30} 1,15-diol (Table S3).
257 However, these correlations are weaker than the ones obtained from Sevilla-Tablada and
258 Madrid-Retiro observatories. These observatories registered longer and more reliable
259 temperature data than those obtained in Granada observatories, which are likely biased
260 by the quality of the reconstructed temperature data. Therefore, after testing the
261 correlations between LCDs and different low elevation observatories (Table S3), we
262 decided to develop the LCD-based temperature calibrations against the temperature time-
263 series from Sevilla-Tablada and Madrid-Retiro observatories. These observatories show
264 the best correlations with the LCD data, in addition to being the most reliable and longest
265 temperature time-series in the region (see Table S3 for further explanations and Fig. 1a
266 for the location of these low-elevation observatories).

267

Another question to clarify in the study records before selecting the reference temperature time-series for the LCD calibration is the potential seasonal effect on the LCD distributions, since different studies have shown diverse relationships between annual or seasonal temperatures and the LCDs. For example, good correlations have been found in marine environments between the fractional abundances of LCDs (expressed as LDI in all the cases) and annual (Rampen et al., 2012), winter and annual (Smith et al., 2013), or autumn and annual sea surface temperatures (Lattaud et al., 2018b). Despite fewer studies on the LCD distribution in freshwater environments, Rampen et al. (2014a) found a good correlation between the LCD distributions in a suite of lake surface sediments and mean summer lake temperatures (deduced from GDGTs). Nevertheless, the direct correlation between these LCD distributions and annual or seasonal air temperatures was weaker, probably due to the location of the weather observatories with respect to each study area. Villanueva et al. (2014) also investigated this seasonal effect and detected changes in the LCD distribution throughout the year in the water column and surface sediments from an African lake that could be either related to successive and different LCD-producer blooms or seasonal variations in the LCD production by a unique source. Both scenarios might affect LCD-based temperature reconstructions.

285

Considering all these constrains to select the best temperature time-series to establish an accurate LCD-based temperature calibration, the most rigorous approach for the studied alpine site would consider annual and monthly water and/or air temperatures of the catchment basin at 3020 masl, as well as, the periods of the year when the LCDs are produced, but these data are not available so far. Thus, the effect of seasonality has been estimated by means of the comparison with reliable seasonal long temperature time-series from lower elevation sites. In this regard, seasonal air temperatures for the last ~100 years registered in Madrid and Sevilla observatories correlate with the LCD distributions (with a weaker correlation for the C_{30} 1,15-diols) and the LDI ($0.9>r>0.6$; $p<0.001$). Nevertheless, this correlation is generally lower than the one obtained when considering only mean annual air temperatures (MAAT) (i.e., in the case of the LDI *vs* MAAT $r=0.9$; $p<0.0001$). Since warm temperatures influence the algae growth in the studied area (Carrillo et al., 1991; Sánchez-Castillo, 1988), we would expect a higher correlation between LCDs and mean seasonal air temperatures from the warmer months (MWAT: May-September), which is potentially the LCD production season, but this correlation is

301 lower than the annual ones in the case of the LDI (LDI vs MWAT $0.8 > r > 0.7$; $p < 0.0001$)

302 (Table S3, S4). A similar pattern is observed when annual and warm season temperatures

303 are compared with the fractional abundances of the C_{28} 1,13-, C_{30} 1,13-, C_{30} 1,15-, and

304 C_{32} 1,15-diols (Table S3). Consequently, in view of 1) the fact that this is the first attempt

305 at a freshwater LCD-based temperature calibration in this area; 2) there exists a high

306 correlation between the different instrumental time-series of regional air temperatures

307 (seasonal vs annual), and 3) the best correlations (normal and detrended) between the

308 LCD distributions and temperatures are obtained when using MAAT (Tables S3, S4), we

309 use MAAT for the LCD-based temperature calibrations in this study. Nevertheless,

310 further work, including a monitoring program for monthly air temperatures in the

311 catchment area and water temperatures in the lake as well as suspended particulate matter

312 and sediment trap studies, is required to better understand the local LCD production,

313 improve the LCD-based temperature calibration, and minimise the uncertainties of the

314 current approach.

315

316   Two groups of reference temperature time-series at 3020 masl, based on the same

317 batch of data, have been estimated in order to overcome the scarcity of high-elevation

318 temperature time-series in the Sierra Nevada and obtain a reliable mean LCD-based

319 temperature calibration: 1) based on the elevational gradient between low and high

320 elevation observatories and 2) based on the direct correlation between temperature time-

321 series from Madrid and Sevilla observatories and that at 3020 masl (Cetursa 5

322 observatory) in the Sierra Nevada, which is near LdRS and at the same elevation (Table

323 S1).

324

325   Reference temperature time-series 1: The environmental lapse rate

326 ($\Delta_{temperature}/\Delta_{elevation}$ in °C/m) between lower elevation observatories (with long

327 temperature time-series: Granada, Sevilla, and Madrid) and those from Sierra Nevada at

328 higher elevation (with shorter temperature time-series: Albergue, and Cetursa 1, 3 and 5)

329 has been estimated in order to correct the elevational gradient between them (more than

330 2200 m: Table S1). Due to few annual data points from high elevation sites, monthly and

331 annual (twelve continuous months) environmental lapse rates were calculated to compare

332 both datasets. The calculated temperature shifts between the reference low elevation

333 observatories and LdRS site at 3020 masl, worked out from Fig. S1 equations (Table S5),

334 was applied to the temperature time-series from Madrid and Sevilla for the last ~100 years

335   in order to obtain two reference temperature reconstructions (from 1908 to 2008 CE) at

336   3020 masl: reference temperature time-series 1a (from Madrid data), and reference

337   temperature time-series 1b (from Sevilla data).

338

339   Reference temperature time-series 2: The direct comparison between Madrid and

340   Sevilla temperatures and those from the observatory Cetursa 5 (3020 masl) by means of

341   ordinary least square regressions has given rise to two equations (Fig. S2a and b) that

342   allow the reconstruction of temperature time-series at 3020 masl from 1908 to 2008:

343   reference temperature time-series 2a (from Madrid data), and reference temperature time-

344   series 2b (from Sevilla data).

345

346   As a result, we have obtained four reference temperature time-series at 3020 masl

347   where the effect of the altitudinal difference between low elevation observatories (Madrid

348   and Sevilla) and LdRS have been corrected by two different methods. Consequently,

349   these four reference temperature series are highly similar, showing a certainly high

350   correlation ($r>0.98$; $p<0.0001$), without significant difference between the sample

351   medians (deduced from a Kruskal-Wallis test), and very low standard deviation between

352   samples from the same time interval (SD<0.2).

353

354   **3. Results**

355

356   **3.1. Long chain diols in the LdRS records**

357

358   Six main LCD isomers have been identified and relative abundance analysed in

359   the LdRS cores: C_{28} and C_{30} 1,13-diols, C_{28} and C_{30} 1,14-diols, and C_{30} and C_{32} 1,15-

360   diols. The LCD abundance changes through time in both records, but the C_{32} 1,15-diol is

361   the predominant isomer in most of the samples. Nevertheless, the relative abundance of

362   the C_{32} 1,15-diol drops abruptly (relative abundances between 25% and 40%) during the

363   LIA, contrasting with a relative increase in the C_{28} and C_{30} 1,13-diols (Fig. 2). This switch

364   in the most abundant isomers can be read as either a change in the LCD producers or an

365   adaptation to colder temperatures of the same organism, and thus affecting the LCD

366   production. Conversely, the C_{28} and C_{30} 1,14-diols show the lowest relative abundances

367   (1.3 ± 0.4% and 1.8 ± 0.3%, respectively), and were only quantified in the short core to

368   assess their potential application as paleothermometer in LdRS. Although they show a

369   good correlation with temperatures (C_{28} 1,14-diol: $0.66 > r > 0.45$ $p < 0.04$; C_{30} 1,14-diol: -

370     $0.82 < r < -0.53$ $p < 0.02$), their low relative abundance, very close to the detection limit,

371   together with a different biological source (Sinninghe Damsté et al., 2003), preclude us

372   from including them in the temperature calibration, and therefore, in the discussion of

373   this study. Consequently, the interpretations in this paper are only focused on the

374   distribution pattern of the relative abundances of the main LCDs in LdRS: C_{28}-C_{30} 1,13-

375   diols and C_{30}-C_{32} 1,15-diols.

376

377   The relative abundances of these four isomers in LdRS correlate well in both short

378   and long cores; only the C_{30} 1,15-diol shows weaker correlations with the other isomers

379   (Table S6). Overall, the C_{28} and C_{30} 1,13-diols show opposite trends to those from the C_{30}

380   and C_{32} 1,15-diols. Their general trends for the last ~100 years seem to be influenced by

381   the temperature oscillations at 3020 masl (Table S7): the C_{28} and C_{30} 1,13-diols display a

382   negative correlation with temperatures ($r < -0.7$ $p < 0.0001$) and the C_{32} 1,15-diol a positive

383   one ($r > 0.8$ $p > 0.0001$). Although the C_{30} 1,15-diol also shows a positive relationship with

384   temperatures, this correlation is weak ($r > 0.3$ $p > 0.0001$). Accordingly, the LDI values

385   from LdRS for the last ~100 years show a significant correlation ($r > 0.9$ $p > 0.0001$) with

386   the reference temperature time-series at 3020 masl (Table S7).

387

388   The different diol isomers in LdRS also show good agreement with the general

389   temperature trends for southwestern Europe during the last ~1500 years (Abrantes et al.,

390   2005; Luterbacher et al., 2016; Nieto-Moreno et al., 2013; Sicre et al., 2016, among

391   others). The C_{30} and C_{32} 1,15-diols depict a positive relationship with temperatures,

392   whereas the C_{28} and C_{30} 1,13-diols display a negative one. Thus, the LDI record obtained

393   from the C_{28}-C_{30} 1,13-diols, and C_{30} 1,15-diol also show important fluctuations during

394   the last ~1500 years, in agreement with the general temperature trends of the Common

395   Era (CE). More specifically, LDI values in the LdRS lgc range from ~0.23 to 0.05 from

396   ~400 to 1900 CE, with maximum and minimum values recorded at ~930 and ~1690 CE,

397   respectively (Fig. 3). These changes are coeval with the minimum temperatures of the

398   LIA and the maximum temperatures of the Medieval Climate Anomaly (MCA) in Europe

399   (e.g., Luterbacher et al., 2016; Nieto-Moreno et al., 2013; Sicre et al., 2016). The rates

400   of change were higher during the 20th century, with LDI values ranging from 0.10 to 0.31

401   in the lowest resolution LdRS lgc record and from 0.13 to 0.32 in the highest resolution

402   LdRS shc record. These minimum and maximum values were reached in both cases

403   during the first and last decades of the 20th century, respectively (Fig. 3).

404

405   **3.2. LCD temperature calibration**

406

407   A total of twenty-six samples from both short and long LdRS cores ranging in age

408   from 1908 to 2008 were selected to perform the LCD-based temperature calibration,

409   along with the two groups of reference temperature time-series at 3020 masl. Since

410   sedimentary samples used in the calibration have a time averaging between 5 and 7 years,

411   a mean of the historical temperatures covering the same time averaging of each sample

412   was calculated.

413

414   Eight different calibrations have been performed: five using the LDI, one using a

415   multiple linear regression of the relative abundances of the C_{28} 1,13-diol, C_{30} 1,13-diol,

416   and C_{30} 1,15-diol (following Rampen et al., 2014a) (MLR calibration 1 hereafter), one

417   using multiple linear regressions of the ratios of the relative abundances of LCDs with

418   positive (even weak) correlation with temperature against the ones with negative

419   correlation (C_{30} 1,15- / C_{28} 1,13-diols; C_{30} 1,15- / C_{30} 1,13-diols; C_{32} 1,15- / C_{28} 1,13-

420   diols; and C_{32} 1,15- / C_{30} 1,13-diols) (MLR calibration 2 hereafter), and one using

421   multiple linear regressions of the ratios of the relative abundances of the C_{30} 1,15- / C_{28}

422   1,13-diols and C_{30} 1,15- / C_{30} 1,13-diols (MLR calibration 3 hereafter). The statistics and

423   the equations for the MLR calibrations 1, 2, and 3 are described in the Table S8.

424

425   In the case of the LDI, ordinary least square regressions were run between the four

426   reference temperature time-series at 3020 masl and the LDI record from LdRS shc and

427   lgc, resulting in four calibration equations (Fig. S3). The slopes of these four equations

428   range from 8.2 to 10.2. The LDI-derived temperatures from the reference time-series 2

429   show the highest values for the last ~100 years, whereas the minimum values are mainly

430   shown by the ones calculated with the reference time-series 1. The difference between

431   the four LDI-derived temperatures for the last ~100 years is low, with a standard deviation

432   lower than 0.13. The standard error of these four individual calibrations ranges from 0.18

433   to 0.23ºC, and the maximum residual is ~0.8ºC. However, due to the uncertainty of

434   establishing an accurate temperature time-series at 3020 masl, LDI-derived temperature

435   values from these LDI individual calibrations have been used to determine the range of

436   the variation (minimum and maximum temperature values) for each point, and an

437   additional calibration, summarising the relationship between LDI and the four reference

438   temperatures at 3020 masl has been performed. The obtained 104 combinations of LDI

439   and temperature data provided an equation representing the average relationship between

440   MAAT and LDI (Eq. (2); Fig. 4a). Since this is a summary of the four temperature time-

441   series, the residual errors include the residual errors of the individual LDI calibrations

442   (Fig. S3). The residual errors of this average temperature calibration, according to both

443   the LDI-reconstructed temperatures and the reference temperature time-series, are lower

444   than 0.8ºC (similar to the four individual LDI calibrations), with the standard error of

445   0.28ºC. The histogram showing the frequency of the residuals reveals that the ~85% of

446   the residuals range from 0.4 to -0.4ºC. This percentage is slightly lower (~62%) when the

447   residual interval is established between 0.2 and -0.2ºC (Fig. 4b). Only one data point from

448   1973 among the 104 data combination may be an outlier since it shows a residual 2.5

449   times higher than the residual standard deviation.

450

451   Equation (2) MAAT (ºC) = 9.147 x LDI - 0.243   (n = 26 x 4; $r^2 = 0.79$)*

452   * n = 26 LDI values plotted against four reference temperature time-series providing a

453   total of 104 combinations.

454

455   All the calibrations (LDI and MLR calibration 1, 2, and 3) show good correlation

456   with temperatures (Fig. 4 for LDI and Table S8 for MRL calibrations 1, 2, and 3). The

457   obtained temperatures from the average LDI calibration and those using multiple linear

458   regressions depict very similar trends in both cores (Fig. S4; $r > 0.96$; $p < 0.0001$).

459   Nevertheless, the correlation is slightly weaker ($r > 0.82$; $p < 0.0001$) for the results from

460   MLR calibration 1 in the long core. In addition, some inconsistencies come up in the

461   reconstructed temperatures from MLR calibration 1: in general, temperatures tend to be

462   lower than those from the other calibrations, giving rise to negative annual values during

463   the LIA. This would be highly unlikely since under this scenario the lake would have

464   stayed frozen all year round, with little or no sedimentation occurring. Temperature

465   reconstructions using MLR calibrations 2 and 3 take the advantage of the ratios of isomers

466   with positive *vs* negative relationship with temperatures. The results are similar to the

467   ones obtained with the LDI, except for the LIA. Nevertheless, we discarded MRL

468   calibration 2 as it also uses the C_{32} 1,15-diol, whose relationship with temperature is not

469   clear, only reporting a positive correlation in some culture studies (Rampen et al., 2014b).

470   MRL calibration 3 provides the most similar results to those from the LDI, especially

471   comparing the temperature anomalies of both records with respect to the last 30 years of

472   the record, showing differences of less than ~0.1ºC. However, this difference increases

473   (~0.3ºC) in the LIA. As this is the first study of LDI in sedimentary records from alpine

474   lakes of the Sierra Nevada area, we have opted for a conservative solution following the

475   LDI temperature calibration. The temperature reconstructions from MRL calibration 1,

476   2, and 3 will only be mentioned when needed in the discussion.

477

478   The application of the obtained calibration to the LDI values of LdRS (Eq. 2)

479   produced the first temperature reconstruction for the Common Era in this alpine area (Fig.

480   3). Nevertheless, a potential challenge of using this kind of down-core proxy calibrations

481   is that the uncertainty of the reconstructed variables (temperature in this case) would

482   increase when data fall outside the calibration data-set (e.g., during the LIA). Further

483   studies on the local LCD production in this alpine area will contribute to extend the range

484   of temperatures in the calibration, reducing the uncertainties of the LCD-derived

485   temperatures.

486

487   In order to estimate the real magnitude of temperature variations during the

488   Common Era, the mean annual air temperature anomaly (MAATA ºC) has been

489   calculated with reference to the annual MAAT of the last 30 years of the record (2008-

490   1979). The lowest temperatures were recorded between ~1600 and ~1780 CE, with a

491   temperature anomaly ranging from ~ -1.9 to ~ -2.2ºC. These temperature anomalies only

492   reached positive values after 1998 (Fig. 3).

493

494   **4. Discussion**

495

496   **4.1. Long chain diol distribution in alpine lakes from southern Iberia**

497

498   The distribution pattern of the main LCDs in LdRS (C_{28}, C_{30} 1,13- and C_{30}, C_{32}

499   1,15-diols) could help us decipher the potential biological producers. There is a high

500   percentage of the C_{32} 1,15-diol, which is one of the main features observed in freshwater

501   environments (Lattaud et al., 2018a; Rampen et al., 2014a) (Fig. 2, S5). Another relevant

502   feature of the distribution of the LCDs in LdRS is the low and constant relative abundance

503   of the C_{30} 1,15-diol (6.5 ± 1.5%) throughout the LdRS records (Fig. 2), agreeing with the

504   range of the most probable distribution of the C_{30} 1,15-diol in marine algae (Fig. S5;

505   Table S9). This feature is not common in marine or lake sediments (de Bar et al., 2016;

506   Lattaud et al., 2017a; Rampen et al., 2014a), resulting in an almost unique area for LdRS

507   isomers (most specifically C_{28} 1,13-, C_{30} 1,15-, and C_{32} 1,15-diols) when comparing with

508   literature data in a ternary diagram (Fig. 2). Conversely, the distribution of both C_{28} and

509   C_{30} 1,13-diols usually shows similar patterns as other freshwater samples (Lattaud et al.,

510   2018a; Rampen et al., 2014a) (Fig. 2, S5, Table S9). A Kruskal-Wallis ANOVA test was

511   used to assess whether the distribution of the main LCDs in LdRS and from other sources

512   (e.g., marine, freshwater, algal culture) were statistically different. Results point towards

513   no significant differences between the whole LCD distribution in LdRS and the other

514   sources. Nevertheless, the Kruskal-Wallis test found significant differences among

515   individual isomers of the different sources (including LdRS). Subsequently, a Mann-

516   Whitney U test was performed to compare pair of groups (individual isomers from LdRS

517   *vs* individual isomers from source 1, 2, and so on), finding significant differences among

518   most of them (Table S9). All these evidences suggest that the LCD distribution in the

519   LdRS might differ from those of previous studies published to date and the potential

520   biological producers at LdRS would be thus uncertain.

521

522   Eustigmatophyceae algae (e.i. *Vischeria* sp., *Eustigmatos* sp.) have been

523   commonly proposed as the main diol producers in freshwater environments dominated

524   by a mix of the C_{28} 1,13-, C_{30} 1,15-, and C_{32} 1,15-diols (Rampen et al., 2014a; Villanueva

525   et al., 2014; Volkman et al., 1999). Moreover, a dominance of the C_{32} 1,15-diol has been

526   identified in families of Goniochloridaceae and Monodopsidaceae (Lattaud et al., 2018a;

527   Rampen et al., 2014a). Nevertheless, planktonic algae communities are very simple in the

528   alpine Sierra Nevada wetlands (Sánchez-Castillo, 1988) and Eustigmatophyceae algae

529   have not been identified so far (Barea-Arco et al., 2001; Sánchez-Castillo, 1988). Thus,

530   this study suggests that LCD producers in LdRS might be different from those identified

531   previously in other freshwater environments and algal culture studies, making the

532   potential source of LCDs even more complex than originally thought. Consequently, the

533   outcomes of this paper (i.e., the LCD-based temperature calibration) should not be

534   generally applied to other freshwater records unless they show a similar LCD distribution

535   as LdRS. Additional research combining lipids and 18S rRNA gene sequencing analyses

536 from suspended particulate matter, surface sediments, and sediment traps would be
537 needed to unravel the real biological sources of LCDs in these alpine wetlands.
538

4.2. LdRS record in the environmental context of the Iberian Peninsula during the
540 **Common Era**
541

542   Abrupt changes in temperature and precipitation have been depicted during the
543 last 2000 years in the Iberian Peninsula and surrounding marine areas (Moreno et al.,
544 2012; Sánchez-López et al., 2016). Precipitation was highly variable, showing arid
545 conditions during the MCA, especially in southern Iberia, overall humid conditions
546 throughout the LIA (with a complex internal structure showing large variability in
547 humidity and extreme events), and arid conditions for the Industrial Period (Moreno et
548 al., 2012; Oliva et al., 2018; Rodrigo et al., 1999; Sánchez-López et al., 2016), especially
549 in high elevation wetlands from southern Iberia (Anderson et al., 2011; Garcia-Alix et al.,
550 2017; Jiménez-Espejo et al., 2014).
551

552   Although the Early Middle Ages displayed a great temperature variability in the
553 Iberian Peninsula and surrounding marine sites (Moreno et al., 2012; Sánchez-López et
554 al., 2016), three main stages have been identified for the last millennium deduced from
555 different proxies: a warm period throughout the MCA followed by cold temperatures
556 during the LIA, ending in an abrupt warming in the second half of the 20th century
557 (Moreno et al., 2012; Oliva et al., 2018; Sánchez-López et al., 2016). One of the proxies
558 used to reconstruct such temperature variations in continental areas of the Iberian
559 Peninsula has been tree ring data. Long tree ring temperature archives of the Iberian
560 Peninsula showed the same overall variations as the ones registered in LdRS, such as high
561 temperatures before 1250 CE (Büntgen et al., 2017), some temperature declines coeval
562 with solar minima during the LIA (e.g., the end of Spörer or Maunder Minima), as well
563 as a period of moderate-low temperatures from ~1850 to ~1940, followed by an
564 increasing temperature trend in the second half of the 20th century with several
565 temperature drops between ~1960 and ~1990 (Büntgen et al., 2017; Tejedor et al., 2017).
566 Nevertheless, the warming documented from the LCD-derived temperatures in the last
567 stages of the LIA is more pronounced in the LdRS record. The same overall trends have
568 been observed in European summer temperatures deduced from tree ring records
569 (Luterbacher et al., 2016) (Fig. 5b, d, and 6b, c). Surprisingly, tree ring data from the

570 Pyrenees and other Iberian areas show minor temperature variations, and even a slight
571 temperature decrease from ~2000 to 2008 similar to the one observed in the LCD-derived
572 temperatures from the LdRS record (Fig. 4c). This temperature stabilization at the
573 beginning of the 21st century is coeval with globally reduced warming rates over the
574 2001–2014 period (Fyfe et al., 2016).

575

576   Contrasting with these continental temperature reconstructions, high-resolution
577 sea surface temperature (SST) estimations from marine sites surrounding the Iberian
578 Peninsula, such as those derived from alkenones ($U^{K'}_{37}$) in the Tagus Delta (Iberian
579 Atlantic Margin) or in the Balearic Islands (western Mediterranean Sea), showed a
580 general decreasing trend for the last ~2000 years, with a warm MCA, a cold LIA, and
581 cold/moderate temperatures for the Industrial Period that do not appear to mirror the
582 modern global warming observed throughout the 20th century (Abrantes et al., 2005;
583 Moreno et al., 2012). Only high-resolution $U^{K'}_{37}$-and TEX$_{86}$-derived (from GDGTs) SST
584 records of the cores 384B and 436B from the Alboran Sea (Nieto-Moreno et al., 2013)
585 and the $U^{K'}_{37}$-SST record of core Gol-Ho1B from the Gulf of Lion (Sicre et al., 2016)
586 have shown a clear temperature increase during the 20th century, similar to the LDI
587 temperature record in LdRS (Fig. 5a,d, 6a,c). The observed heterogeneity in the SST
588 reconstructions based on different biomarkers such as alkenones (Abrantes et al., 2005;
589 Moreno et al., 2012; Rodrigo-Gámiz et al., 2014), GDGTs (Nieto-Moreno et al., 2013) or
590 LCDs (Rodrigo-Gámiz et al., 2014) could be explained since each record belongs to a
591 different biogeographical area influenced by specific temporal and dynamic
592 oceanographic regimes, as well as by different primary productivity patterns of each
593 biological source (e.g., seasonality or bloom length) (Sicre et al., 2016).

594

595   The previously described climate variability in precipitation and temperature
596 during the last ~1500 years in the Iberian Peninsula have been explained by different
597 forcing mechanisms such as the effect of the westerlies-North Atlantic climate dynamics,
598 internal climate variability, solar irradiance, volcanism, or anthropogenic forcing
599 (Gómez-Navarro et al., 2011; Gómez-Navarro et al., 2012; Moreno et al., 2012; Sánchez-
600 López et al., 2016). Their potential effect on the LCD distribution in the LdRS records is
601 discussed in the following section.

602

4.3. Control mechanisms on alpine temperatures in SW Europe during the Common Era

This discussion is based on the LDI-temperature reconstruction. However, similar results are obtained when comparing the temperature reconstructions from MLR calibrations 1, 2, and 3 in LdRS and the different forcing mechanisms assessed in this section (Tables S10-S13).

Solar, volcanic, and anthropogenic (e.g., CO_2 and CH_4) radiative changes, along with the internal variability are usually attributed as the leading factors controlling temperatures during the Common Era (Ammann et al., 2007; IPCC, 2013). In addition, North Atlantic climate dynamics such as the North Atlantic Oscillation (NAO) or the Atlantic Multidecadal Oscillation (AMO) are other potential drivers of natural climate variability in the Iberian Peninsula (López-Moreno et al., 2011; Moreno et al., 2012; O'Reilly et al., 2017; Sánchez-López et al., 2016). The control of the North Atlantic climate dynamics in the studied alpine wetlands is evident, at least for precipitation and humidity fluctuations, since the NAO and solar forcing have been described as the main controls on the paleoenvironmental evolution recorded in this area (Garcia-Alix et al., 2017; Ramos-Román et al., 2016). Conversely, other studies have shown that the NAO climate mode had little effect on temperatures in this alpine area from 1950 to 2006 CE (López-Moreno et al., 2011). LdRS data agree with this observation, since no correlation (Tables S10-S13) has been detected between the NAO reconstruction (Trouet et al., 2009) and the obtained LCD record for the last millennium. The AMO has an impact on the North Atlantic atmospheric blocking mechanisms (Häkkinen et al., 2011) and on the European and Mediterranean temperatures, especially during the AMO warm phases (O'Reilly et al., 2017). In the study area, the AMO shows a moderate long-term correlation (Figs. 5d,e and 6c,d $r>0.60$; $p<0.01$) with both long and short core derived-LDI records, but the correlation decreases when long-term trends are removed ($r<0.32$; $p>0.1$) (Tables S10, S11). Since the nature of the AMO and its specific drivers are still a matter of debate, i.e., internal ocean variability control (multidecadal fluctuations in the Atlantic Meridional Overturning Circulation) versus solar or volcanic forcing for the last centuries (Knudsen et al., 2014), we cannot conclude whether the observed correlations represent the sole effect of the AMO or the influence of its underlying forcing mechanisms.

637

638   The significant correlation at long and short terms ($r>0.61$; $p<0.005$) between
639 LDI-derived temperatures from LdRS records and greenhouse gases (Schmidt et al.,
640 2011) (Fig. 6c, g; Table S10), especially since the beginning of the 20th century (Industrial
641 Period) (Fig. 5d,g; Table S11), suggests that greenhouse gases might have an important
642 effect on temperatures at this high elevation site.

643

644   The potential impact of solar radiation and volcanic eruptions on climate over both
645 short- and long-time scales is a topic of controversy in the literature (Ammann et al.,
646 2007). In this regard, volcanic forcing, which should give rise to negative radiative
647 forcing in the climate system (Ammann et al., 2007; Sigl et al., 2015), do not show a
648 significant correlation with LDI-derived temperatures from LdRS records over the last
649 1500 years (Figs. 5d,h and 6c,h; Table S10, S11). We suggest that this lack of influence
650 at LdRS records is a function of its high-altitude location, at 3020 masl, in the free
651 troposphere, which reduces the environmental impact of small volcanic tropospheric
652 eruptions that likely have greater effects on lower elevation sites (Mather et al., 2013). In
653 addition, the relatively short residence time of volcanic aerosols in the atmosphere mainly
654 causes, at most, decadal-timescale effects (Sigl et al., 2015) that can be difficult to identify
655 in most sedimentary records due to the age resolution, as in the case of older sediments
656 than 200 years in LdRS. Nevertheless, large explosive volcanic eruptions delivering large
657 amounts of stratospheric aerosols (Marotzke and Forster, 2015; Sigl et al., 2015), such as
658 that for Agung Volcano in Bali, Indonesia (1963-1964 CE), may be associated with a
659 small depression in LDI-derived temperatures observed in LdRS records (Fig. 5d,h).
660 Although cold LDI-reconstructed temperatures occasionally seem to occur coevally with
661 volcanic eruptions, for example, 560-510 and 320 years ago (~1450-1500 and 1690 CE)
662 (Sigl et al., 2015), there is no consistent relationship between the intensity - number of
663 large eruptions and the reconstructed coolings in LdRS records, especially over the last
664 ~200 years when the sample resolution would be enough to detect them (LdRS shc).

665

666   Most of the above-mentioned cooling events recorded in LdRS, such as those
667 during the LIA, are coeval with low solar activity periods like the Spörer Minimum (from
668 ~1450 to 1550 CE) or the Maunder Minimum (from ~1645 to 1715 CE) (Stuiver and
669 Quay, 1980) (Fig. 6). Thus, long-term correlations between LDI-derived temperatures
670 and solar activity, based on reconstructions of the solar irradiance and cosmogenic

671   isotopes (such as ^{14}C), are evident during the last ~1500 years in LdRS record ($r>0.69$; p

672   <0.002) (Fig. 6c,e,f; Table S11). This correlation drops ($0.37< r <0.56$ and $0.04< p <0.14$)

673   when long-term trends are removed (Table S11). The long-term solar influence agrees

674   with previous observations in other alpine records of this area (Garcia-Alix et al., 2017;

675   Ramos-Román et al., 2016). Solar activity slightly decreases its long-term influence in

676   LdRS record during the last ~200 years ($r>0.56$; $p<0.001$) and disappears when long-term

677   trends are removed (Table S10). Only some occasional temperature decreases or slower

678   rates of warming such as during the 19th to 20th century transition, from ~1930 to 1940,

679   from ~1960 to 1975, and around 1988 CE, are coeval with slight declines in the total solar

680   activity (Fig. 5d,f: blue arrows).

681

682   In the same way, LdRS registered a small decrease in LDI-derived temperatures

683   (or stabilization) at the beginning of the 21st century (Fig. 5d), also recorded in the Madrid

684   and Sevilla temperature time-series (Spanish National Weather Agency - AEMet Open

685   Data, 2019), and thus in the reconstructed reference temperatures time-series at 3020 masl

686   (Fig. 5c), in tree ring records of the the Pyrenees and Iberian Range (Büntgen et al., 2017;

687   Tejedor et al., 2017), in marine platforms of the western Mediterranean (Fig. 5a) (Sicre

688   et al., 2016), and globally (Fyfe et al., 2016). Although this slowdown agrees with a

689   decreasing trend in solar activity and a slight stabilization of atmospheric methane

690   concentrations (Fig. 5f,g), the causes are more complex, and probably related to a

691   combination of internal variability and radiative forcing (e.g., volcanic and solar

692   activity, or decadal timescale changes in anthropogenic aerosols) (Fyfe et al., 2016).

693

694   **4.4. Exceeding natural thresholds in alpine areas**

695

696   The LDI-derived temperatures from LdRS exceeded the highest pre-industrial

697   temperatures in the early 1950s (Fig. 6c), under full anthropogenic influence. The

698   comparison between pre-industrial and post-industrial scenarios in the study site

699   highlights the human impact on natural trends. In this regard, the temperature increase

700   during the last stages of the LIA (from ~1690 to ~1850 CE), an analogue for a non-

701   anthropogenic temperature-increase scenario, was between ~1.2 and ~1.4ºC

702   (~0.09ºC/decade; Fig. 6), whereas the mean temperature rise throughout the 20th century

703   was ~1.8ºC (~0.18ºC/decade; Fig. 7). Both warming rates are roughly similar to those

704 reconstructed from MLR calibrations 1, 2, and 3: ~0.06-0.09ºC/decade for the last stages

705 of the LIA, and ~0.17-0.18ºC/decade for the 20th century. Although this means that on

706 average, the warming rate was two times faster throughout the 20th century than at the

707 end of the LIA (Fig. 7), these observations are based on a low sample density for the LIA

708 (8 samples), which might slightly increase the uncertainty for this period. By comparison,

709 average global temperatures rose by ~0.85ºC from 1880 to 2012 CE, corresponding to

710 0.06ºC/decade (IPCC, 2013), which highlight the high-elevation amplification effect of

711 temperatures on this vulnerable area.

712

713   Other European alpine areas in the Mediterranean region, such as those from the

714 Alps, experienced a slower warming rate during the 20th century (~0.11ºC/decade) (Fig.

715 7) (Auer et al., 2007; Böhm et al., 2010). This is ~1.6 times slower than the warming rate

716 recorded in the Sierra Nevada. This evidence, along with the generally smaller amount of

717 precipitation in the alpine areas of the western Mediterranean region (Auer et al., 2007;

718 Rodrigo et al., 1999), allows us to conclude that the 20th century environmental stress in

719 this area was greater than in the Alps.

720

721   Future scenarios are not optimistic for Sierra Nevada since temperatures at ~1000

722 masl may rise between 2.2ºC and 5.3ºC by the end of the 21st century (Pérez-Luque et al.,

723 2016), exceeding the global projections of the IPCC-2013 report (IPCC, 2013). However,

724 temperature projection and its subsequent impact on alpines areas of the Sierra Nevada

725 have not been satisfactorily assessed so far due to the lack of long-term quantitative

726 climatic records at these elevations (e.g., temperature). The LCD-based temperatures at

727 ~3000 masl will solve this lack of quantitative data and will be valuable to project future

728 scenarios in these alpine ecosystems where endemic and endangered species inhabit

729 (Blanca, 2001; Munguira and Martin, 1993).

730

731 **4.5. Impact on the southwesternmost European alpine glaciers**

732

733   The studied alpine area supported the southernmost glaciers in Europe during the

734 LIA. Glaciers and permanent snow fields below ~3000 masl, such as those of Corral del

735 Mulhacen (~2950 masl) whose last mention in the literature was between 1809 and 1849

736 CE (Oliva and Gomez-Ortiz, 2012), would have totally disappeared by the decrease in

737 regional precipitation during the first half of the 19th century (Rodrigo et al., 1999). The
738 climatic features at the end of the 19th century and the beginning of the 20th century did
739 not allow this glacier to re-establish itself (Fig. 8). Post-LIA climatic conditions have also
740 been proposed as the trigger for the melting of the Corral del Veleta Glacier in Sierra
741 Nevada (~3100 masl) at the beginning of the 20th century (Garcia-Alix et al., 2017; Oliva
742 and Gomez-Ortiz, 2012; Oliva et al., 2018). However, the LCDs in LdRS records show
743 that reconstructed temperatures did not exceed the levels of the 1850s until the late 1940s
744 CE. Precipitation was low in the southern Iberian Peninsula during the first half of the
745 20th century, but similar, and even lower, precipitation values were registered before
746 ~1850 CE (Rodrigo et al., 1999; Spanish National Weather Agency - AEMet Open Data,
747 2019) (Fig. 8). Therefore, how could the glacier have retreated under this almost steady-
748 state scenario? A similar paradox has been described in the Alps (Painter et al., 2013),
749 where glaciers began to sharply retreat after the mid-19th century, even though
750 temperature and precipitation records would suggest that glacier expansion should have
751 occurred at least until the first decades of the 20th century. In this case, one of the proposed
752 triggers for the glacier retreat was the industrial black carbon deposition that amplified
753 the solar radiation absorbed at the snow surface and caused its subsequent melting - not
754 a temperature or precipitation change (Painter et al., 2013). Precipitation data from the
755 southern Iberia (Rodrigo et al., 1999) along with the LCD-reconstructed temperatures in
756 LdRS records suggest that temperature and precipitation were not the only drivers of
757 glacial retreat that led to the melting of permanent glaciers in the Sierra Nevada in the
758 1920s. Instead, mirroring the case of the Alps, it is plausible that other factors reducing
759 the albedo, such as enhanced atmospheric deposition may have played a strong role. In
760 this regard, important atmospheric depositional events have been recorded in the study
761 alpine sites of southern Iberia from the mid-19th century to the first decades of the 20th
762 century caused by both enhanced North African dust fluxes (Mulitza et al., 2010)
763 (Jiménez et al., 2018) as well as a spike in atmospheric pollution (as observed in
764 anthropogenic Pb and Hg records in Sierra Nevada; Fig. 8) (Garcia-Alix et al., 2017;
765 Garcia-Alix et al., 2013). Similarly, both phenomena have been demonstrated as triggers
766 for glacier retreat (Painter et al., 2013) and snow melt in the Alps (Di Mauro et al., 2018).
767
768   Melting of the last glaciated area in the Sierra Nevada during the first decades of
769 the 20st century (Grunewald and Scheithauer, 2010) represents an important turning point
770 regarding recent environmental change in this alpine region (Garcia-Alix et al., 2017;

771 Jiménez et al., 2019). The rapid pace of environmental change in the area after this date
772 is attributed to an amplified effect of warming and aridification (Fig. 8b,c) that increased
773 stress on vulnerable ecosystems (Garcia-Alix et al., 2017; Jiménez et al., 2019; Jiménez
774 et al., 2018) with little hope for return of local glaciers.

775

776 **5. Concluding remarks**

777

778   This study shows the vulnerability of alpine regions and the importance of their
779 monitoring for a better understanding of climate variability and future rapid responses. In
780 this regard, algal-derived biomarkers from LdRS records have given rise to the first long-
781 chain alky diol temperature calibration in freshwater environments by means of the
782 comparison with instrumental temperature time-series. The combination of both short and
783 long sediment cores has provided both a highly accurate LCD-temperature calibration for
784 the instrumental period and a long-term historical perspective on the modern warming.
785 This approach delivers a better time-integrated temperature model than discrete
786 temperature measurements for the 20th century. Nevertheless, the lack of information
787 about the biological sources of LCDs in the Sierra Nevada means that this calibration can
788 only be potentially applied to other lakes with a similar LCD distribution or in the same
789 alpine area.

790

791   The low sample resolution in the longer core before ~1500 CE precludes us from
792 constraining the main natural controls on temperatures in this high-elevation site for the
793 Common Era. However, the general trends support that the presumed primary effect of
794 greenhouse gases on temperatures reconstructed from algal-lipids in this alpine region of
795 southern Iberia is likely modulated by long-term solar forcing. In recent times,
796 greenhouse gases seem to be the major temperature driver in this high elevation site.
797 Volcanic forcing appears to have little effect on reconstructed temperatures in this alpine
798 area. The Atlantic Multidecadal Oscillation (AMO) have also shown to have a long-term
799 effect in the study area; however, due its complex nature, the real effect of the AMO on
800 LCD-reconstructed temperatures in LdRS records cannot be fully constrained. In any
801 case, the effect of the internal climate variability on local temperatures cannot be ruled
802 out. LdRS records also highlight the potential impact that non-climatic environmental
803 drivers such as atmospheric dust and pollution deposition can have exerted on these
804 remote alpine environments (e.g., glacier/snow melting).

805

    Alpine temperatures of southern Iberia exceeded the highest scores reached during pre-industrial times in the 1950s. This means that the rate of warming throughout the 20th century doubled that of the last stages of the LIA. Furthermore, this modern warming rate is higher in the Sierra Nevada than in the Alps, highlighting the important environmental stress in the Sierra Nevada ecosystems. In addition to the amplified effect of warming and aridification, the local environmental pressure may have enhanced throughout the 20th century due to the disappearance of perennial snow fields and the gradual reduction of the seasonal snow cover affecting the local water availability. Future projections suggest that warming in this fragile alpine region will continue at similar rates or even higher than ones registered during the last century.

Data availability. Fractional abundances of the C_{28} 1,13-diol, C_{28} 1,14-diol, C_{30} 1,13-diol, C_{30} 1,14-diol, C_{30} 1,15-diol, and C_{32} 1,15-diol from the studied cores (LdRS shc and LdRS lgc), along with the four reference temperature time-series at 3020 masl from 1908 to 2008 are available online at: https://issues.pangaea.de/browse/PDI-22604

Supplement. The supplement related to this article is available online at:
https://doi.org/

Author contributions. The study was conceived by AG-A and JLT. CPM, LJ, GJM, and RSA recovered the sediment cores. AG-A analysed the samples and processed the data. All co-authors discussed the data and equally contributed to the preparation of the manuscript.

Competing interests. The authors declare that they have no conflict of interest.

Acknowledgements. We would like to thank V. Slaymark (University of Glasgow), for her help preparing and analysing the organic and inorganic samples, as well as F.J. Bonet García, C. González Hidalgo, and M.J. Esteban Parra for providing the temperature time-series from the Sierra Nevada and the South of Spain. We also want to thank the Editor, E. McClymont, and two anonymous reviewers for their useful comments and suggestions that improved the manuscript.

Financial support. This study was supported by the project P11-RNM 7332 of the "Junta de Andalucía", the projects CGL2017-85415-R, CGL2013-47038-R and CGL2011-23483 of the "Ministerio de Economía y Competitividad of Spain and Fondo Europeo de Desarrollo Regional FEDER", the project 87/2007 of the OAPN-Ministerio de Medio Ambiente, as well as the research group RNM-190 (Junta de Andalucía). A.G.-A. was also supported by a Marie Curie Intra-European Fellowship of the 7th Framework Programme for Research, Technological Development and Demonstration of the European Commission (NAOSIPUK. Grant Number: PIEF-GA-2012-623027) and by a Ramón y Cajal Fellowship RYC-2015-18966 of the Spanish Government (Ministerio de Economía y Competividad). J.L.T. hosted the NAOSIPUK project (PIEF-GA-2012-623027) at the University of Glasgow.

References

Abrantes, F., Lebreiro, S., Rodrigues, T., Gil, I., Bartels-Jónsdóttir, H., Oliveira, P., Kissel, C., and Grimalt, J. O.: Shallow-marine sediment cores record climate variability and earthquake activity off Lisbon (Portugal) for the last 2000 years, Quaternary Science Reviews, 24, 2477-2494, 2005.

Ammann, C. M., Joos, F., Schimel, D. S., Otto-Bliesner, B. L., and Tomas, R. A.: Solar influence on climate during the past millennium: Results from transient simulations with the NCAR Climate System Model, Proceedings of the National Academy of Sciences, 104, 3713-3718, 2007.

Anderson, R. S., Jiménez-Moreno, G., Carrión, J., and Pérez-Martinez, C.: Postglacial history of alpine vegetation, fire, and climate from Laguna de Río Seco, Sierra Nevada, southern Spain, Quaternary Science Reviews, 30, 1615–1629, 2011.

Auer, I., Böhm, R., Jurkovic, A., Lipa, W., Orlik, A., Potzmann, R., Schöner, W., Ungersböck, M., Matulla, C., Briffa, K., Jones, P., Efthymiadis, D., Brunetti, M., Nanni, T., Maugeri, M., Mercalli, L., Mestre, O., Moisselin, J.-M., Begert, M., Müller-Westermeier, G., Kveton, V., Bochnicek, O., Stastny, P., Lapin, M., Szalai, S., Szentimrey, T., Cegnar, T., Dolinar, M., Gajic-Capka, M., Zaninovic, K., Majstorovic, Z., and Nieplova, E.: HISTALP—historical instrumental climatological surface time series of the Greater Alpine Region, International Journal of Climatology, 27, 17-46, 2007.

872   Balzano, S., Lattaud, J., Villanueva, L., Rampen, S. W., Brussaard, C. P. D., van

873   Bleijswijk, J., Bale, N., Sinninghe Damsté, J. S., and Schouten, S.: A quest for the

874   biological sources of long chain alkyl diols in the western tropical North Atlantic

875   Ocean, Biogeosciences, 15, 5951-5968, 2018.

876   Barea-Arco, J., Pérez-Martínez, C., and Morales-Baquero, R.: Evidence of a mutualistic

877   relationship between an algal epibiont and its host, Daphnia pulicaria, Limnology

878   and Oceanography, 46, 871-881, 2001.

879   Blanca, G.: Flora amenazada y endémica de Sierra Nevada, Consejería de Medio

880   Ambiente de la Junta de Andalucía and University of Granada, 2001.

881   Böhm, R., Jones, P. D., Hiebl, J., Frank, D., Brunetti, M., and Maugeri, M.: The early

882   instrumental warm-bias: a solution for long central European temperature series

883   1760–2007, Climatic Change, 101, 41-67, 2010.

884   Büntgen, U., Krusic, P. J., Verstege, A., Sangüesa-Barreda, G., Wagner, S., Camarero,

885   J. J., Ljungqvist, F. C., Zorita, E., Oppenheimer, C., Konter, O., Tegel, W.,

886   Gärtner, H., Cherubini, P., Reinig, F., and Esper, J.: New Tree-Ring Evidence

887   from the Pyrenees Reveals Western Mediterranean Climate Variability since

888   Medieval Times, Journal of Climate, 30, 5295-5318, 2017.

889   Carrillo, P., Cruz-Pizarro, L., and Sánchez Castillo, P. M.: Aportación al conocimiento

890   del ciclo biológico de Chromulina nevadensis, Acta Botánica Malacitana, 16, 19-

891   26, 1991.

892   Castañeda, I. S. and Schouten, S.: A review of molecular organic proxies for examining

893   modern and ancient lacustrine environments, Quaternary Science Reviews, 30,

894   2851-2891, 2011.

895   Castillo Martín, A.: Lagunas de Sierra Nevada, Editorial Universidad de Granada,

896   Granada, 2009.

897   Catalan, J., Pla-Rabés, S., Wolfe, A. P., Smol, J. P., Rühland, K. M., Anderson, N. J.,

898   Kopáček, J., Stuchlík, E., Schmidt, R., Koinig, K. A., Camarero, L., Flower, R. J.,

899   Heiri, O., Kamenik, C., Korhola, A., Leavitt, P. R., Psenner, R., and Renberg, I.:

900   Global change revealed by palaeolimnological records from remote lakes: a

901   review, Journal of Paleolimnology, 49, 513-535, 2013.

902   Coddington, O., Lean, J. L., Pilewskie, P., Snow, M., and Lindholm, D.: A Solar

903   Irradiance Climate Data Record, Bulletin of the American Meteorological

904   Society, 97, 1265-1282, 2016.

905 Colcord, D. E., Cadieux, S. B., Brassell, S. C., Castañeda, I. S., Pratt, L. M., and White,
906   J. R.: Assessment of branched GDGTs as temperature proxies in sedimentary
907   records from several small lakes in southwestern Greenland, Organic
908   Geochemistry, 82, 33-41, 2015.
909 de Bar, M. W., Dorhout, D. J. C., Hopmans, E. C., Rampen, S. W., Sinninghe Damsté,
910   J. S., and Schouten, S.: Constraints on the application of long chain diol proxies in
911   the Iberian Atlantic margin, Organic Geochemistry, 101, 184-195, 2016.
912 Di Mauro, B., Garzonio, R., Rossini, M., Filippa, G., Pogliotti, P., Galvagno, M., Morra
913   di Cella, U., Migliavacca, M., Baccolo, G., Clemenza, M., Delmonte, B., Maggi,
914   V., Dumont, M., Tuzet, F., Lafaysse, M., Morin, S., Cremonese, E., and Colombo,
915   R.: Saharan dust events in the European Alps: role on snowmelt and geochemical
916   characterization, The Cryosphere Discuss., 2018, 1-28, 2018.
917 Easterling, D. R., Meehl, G. A., Parmesan, C., Changnon, S. A., Karl, T. R., and
918   Mearns, L. O.: Climate Extremes: Observations, Modeling, and Impacts, Science,
919   289, 2068-2074, 2000.
920 Foster, L. C., Pearson, E. J., Juggins, S., Hodgson, D. A., Saunders, K. M., Verleyen,
921   E., and Roberts, S. J.: Development of a regional glycerol dialkyl glycerol
922   tetraether (GDGT)–temperature calibration for Antarctic and sub-Antarctic lakes,
923   Earth and Planetary Science Letters, 433, 370-379, 2016.
924 Fyfe, J. C., Meehl, G. A., England, M. H., Mann, M. E., Santer, B. D., Flato, G. M.,
925   Hawkins, E., Gillett, N. P., Xie, S.-P., Kosaka, Y., and Swart, N. C.: Making
926   sense of the early-2000s warming slowdown, Nature Climate Change, 6, 224,
927   2016.
928 Gal, J.-K., Kim, J.-H., and Shin, K.-H.: Distribution of long chain alkyl diols along a
929   south-north transect of the northwestern Pacific region: Insights into a paleo sea
930   surface nutrient proxy, Organic Geochemistry, 119, 80-90, 2018.
931 García Montoro, C., Titos Martínez, M., and Casado Sánchez de Castilla, M.: Sierra
932   Nevada. Una expedición al pico de Veleta desde los Baños de Lanjarón (1859),
933   Universidad de Granada, Editorial Universidad de Granada, 2016.
934 Garcia-Alix, A., Jimenez Espejo, F. J., Toney, J. L., Jiménez-Moreno, G., Ramos-
935   Román, M. J., Anderson, R. S., Ruano, P., Queralt, I., Delgado Huertas, A., and
936   Kuroda, J.: Alpine bogs of southern Spain show human-induced environmental
937   change superimposed on long-term natural variations, Scientific Reports, 7, 7439
938   2017.

939 Garcia-Alix, A., Jimenez-Espejo, F. J., Lozano, J. A., Jimenez-Moreno, G., Martinez-
940   Ruiz, F., Garcia Sanjuan, L., Aranda Jimenez, G., Garcia Alfonso, E., Ruiz-
941   Puertas, G., and Anderson, R. S.: Anthropogenic impact and lead pollution
942   throughout the Holocene in Southern Iberia, Science of the Total Environment,
943   449, 451-460, 2013.

944 García-Alix, A., Jiménez-Moreno, G., Anderson, R. S., Jiménez Espejo, F. J., and
945   Delgado Huertas, A.: Holocene environmental change in southern Spain deduced
946   from the isotopic record of a high-elevation wetland in Sierra Nevada, Journal of
947   Paleolimnology, 48, 471-484, 2012.

948 Giorgi, F.: Climate change hot-spots, Geophysical Research Letters, 33, 2006.

949 Gómez-Navarro, J. J., Montávez, J. P., Jerez, S., Jiménez-Guerrero, P., Lorente-Plazas,
950   R., González-Rouco, J. F., and Zorita, E.: A regional climate simulation over the
951   Iberian Peninsula for the last millennium, Clim. Past, 7, 451-472, 2011.

952 Gómez-Navarro, J. J., Montávez, J. P., Jiménez-Guerrero, P., Jerez, S., Lorente-Plazas,
953   R., González-Rouco, J. F., and Zorita, E.: Internal and external variability in
954   regional simulations of the Iberian Peninsula climate over the last millennium,
955   Clim. Past, 8, 25-36, 2012.

956 Gonzalez-Hidalgo, J. C., Peña-Angulo, D., Brunetti, M., and Cortesi, N.: MOTEDAS: a
957   new monthly temperature database for mainland Spain and the trend in
958   temperature (1951–2010), International Journal of Climatology, 35, 4444-4463,
959   2015.

960 Grunewald, K. and Scheithauer, J.: Europe's southernmost glaciers: response and
961   adaptation to climate change, Journal of Glaciology, 56, 129-142, 2010.

962 Häkkinen, S., Rhines, P. B., and Worthen, D. L.: Atmospheric Blocking and Atlantic
963   Multidecadal Ocean Variability, Science, 334, 655-659, 2011.

964 Hansen, J., Ruedy, R., Sato, M., and Lo, K.: Global Surface Temperature Change,
965   Reviews of Geophysics, 48, 2010.

966 IPCC: Climate Change 2013: The Physical Science Basis. Contribution of Working
967   Group I to the Fifth Assessment Report of the Intergovernmental Panel on
968   Climate Change, Cambridge University Press, Cambridge, United Kingdom and
969   New York, NY, USA, 2013.

970 Jiménez, L., Conde-Porcuna, J. M., García-Alix, A., Toney, J. L., Anderson, R. S.,
971   Heiri, O., and Pérez-Martínez, C.: Ecosystem Responses to Climate-Related

972   Changes in a Mediterranean Alpine Environment Over the Last ~ 180 Years,

973   Ecosystems, 22, 563-577, 2019.

974 Jiménez, L., Romero-Viana, L., Conde-Porcuna, J. M., and Pérez-Martínez, C.:

975   Sedimentary photosynthetic pigments as indicators of climate and watershed

976   perturbations in an alpine lake in southern Spain, Limniteca, 34, 439-454, 2015.

977 Jiménez, L., Rühland, K. M., Jeziorski, A., Smol, J. P., and Pérez-Martínez, C.: Climate

978   change and Saharan dust drive recent cladoceran and primary production changes

979   in remote alpine lakes of Sierra Nevada, Spain, Global Change Biology, 28,

980   e139–e158, 2018.

981 Jiménez-Espejo, F. J., García-Alix, A., Jiménez-Moreno, G., Rodrigo-Gámiz, M.,

982   Anderson, R. S., Rodríguez-Tovar, F. J., Martínez-Ruiz, F., Giralt, S., Delgado

983   Huertas, A., and Pardo-Igúzquiza, E.: Saharan aeolian input and effective

984   humidity variations over western Europe during the Holocene from a high altitude

985   record, Chemical Geology, 374-375, 1-12, 2014.

986 Jiménez-Moreno, G. and Anderson, R. S.: Holocene vegetation and climate change

987   recorded in alpine bog sediments from the Borreguiles de la Virgen, Sierra

988   Nevada, southern Spain, Quaternary Research, 77, 44-53, 2012.

989 Jiménez-Moreno, G., García-Alix, A., Hernández-Corbalán, M. D., Anderson, R. S.,

990   and Delgado-Huertas, A.: Vegetation, fire, climate and human disturbance history

991   in the southwestern Mediterranean area during the late Holocene, Quaternary

992   Research, 79, 110-122, 2013.

993 Knudsen, M. F., Jacobsen, B. H., Seidenkrantz, M.-S., and Olsen, J.: Evidence for

994   external forcing of the Atlantic Multidecadal Oscillation since termination of the

995   Little Ice Age, Nature Communications, 5, 3323, 2014.

996 Lattaud, J., Dorhout, D., Schulz, H., Castañeda, I. S., Schefuß, E., Sinninghe Damsté, J.

997   S., and Schouten, S.: The C32 alkane-1,15-diol as a proxy of late Quaternary

998   riverine input in coastal margins, Clim. Past, 13, 1049-1061, 2017a.

999 Lattaud, J., Kim, J.-H., De Jonge, C., Zell, C., Sinninghe Damsté, J. S., and Schouten,

1000   S.: The C32 alkane-1,15-diol as a tracer for riverine input in coastal seas,

1001   Geochimica et Cosmochimica Acta, 202, 146-158, 2017b.

1002 Lattaud, J., Kirkels, F., Peterse, F., Freymond, C. V., Eglinton, T. I., Hefter, J.,

1003   Mollenhauer, G., Balzano, S., Villanueva, L., van der Meer, M. T. J., Hopmans,

1004   E. C., Sinninghe Damsté, J. S., and Schouten, S.: Long-chain diols in rivers:

1005  distribution and potential biological sources, Biogeosciences, 15, 4147-4161,

1006  2018a.

1007 Lattaud, J., Lo, L., Huang, J.-J., Chou, Y.-M., Gorbarenko, S. A., Sinninghe Damsté, J.

1008  S., and Schouten, S.: A Comparison of Late Quaternary Organic Proxy-Based

1009  Paleotemperature Records of the Central Sea of Okhotsk, Paleoceanography and

1010  Paleoclimatology, 33, 732-744, 2018b.

1011 Longo, W. M., Huang, Y., Yao, Y., Zhao, J., Giblin, A. E., Wang, X., Zech, R.,

1012  Haberzettl, T., Jardillier, L., Toney, J., Liu, Z., Krivonogov, S., Kolpakova, M.,

1013  Chu, G., D'Andrea, W. J., Harada, N., Nagashima, K., Sato, M., Yonenobu, H.,

1014  Yamada, K., Gotanda, K., and Shinozuka, Y.: Widespread occurrence of distinct

1015  alkenones from Group I haptophytes in freshwater lakes: Implications for

1016  paleotemperature and paleoenvironmental reconstructions, Earth and Planetary

1017  Science Letters, 492, 239-250, 2018.

1018 López-Moreno, J. I., Vicente-Serrano, S. M., Morán-Tejeda, E., Lorenzo-Lacruz, J.,

1019  Kenawy, A., and Beniston, M.: Effects of the North Atlantic Oscillation (NAO)

1020  on combined temperature and precipitation winter modes in the Mediterranean

1021  mountains: Observed relationships and projections for the 21st century, Global

1022  and Planetary Change, 77, 62-76, 2011.

1023 Luterbacher, J., Werner, J. P., Smerdon, J. E., Fernández-Donado, L., González-Rouco,

1024  F. J., Barriopedro, D., Ljungqvist, F. C., Büntgen, U., Zorita, E., Wagner, S.,

1025  Esper, J., McCarroll, D., Toreti, A., Frank, D., Jungclaus, J. H., Barriendos, M.,

1026  Bertolin, C., Bothe, O., Brázdil, R., Camuffo, D., Dobrovolný, P., Gagen, M.,

1027  García-Bustamante, E., Ge, Q., Gómez-Navarro, J. J., Guiot, J., Hao, Z., Hegerl,

1028  G. C., Holmgren, K., Klimenko, V. V., Martín-Chivelet, J., Pfister, C., Roberts,

1029  N., Schindler, A., Schurer, A., Solomina, O., von Gunten, L., Wahl, E., Wanner,

1030  H., Wetter, O., Xoplaki, E., Yuan, N., Zanchettin, D., Zhang, H., and Zerefos, C.:

1031  European summer temperatures since Roman times, Environmental Research

1032  Letters, 11, 024001, 2016.

1033 Mann, M. E., Zhang, Z., Rutherford, S., Bradley, R. S., Hughes, M. K., Shindell, D.,

1034  Ammann, C., Faluvegi, G., and Ni, F.: Global Signatures and Dynamical Origins

1035  of the Little Ice Age and Medieval Climate Anomaly, Science, 326, 1256-1260,

1036  2009.

1037 Marotzke, J. and Forster, P. M.: Forcing, feedback and internal variability in global

1038  temperature trends, Nature, 517, 565-570, 2015.

1039   Mather, T. A., Pyle, D. M., and Oppenheimer, C.: Tropospheric Volcanic Aerosol. In:
1040   Volcanism and the Earth's Atmosphere, American Geophysical Union, 2013.

1041   Médail, F. and Quézel, P.: Biodiversity Hotspots in the Mediterranean Basin: Setting
1042   Global Conservation Priorities, Conservation Biology, 13, 1510-1513, 1999.

1043   Mesa-Fernández, J. M., Jiménez-Moreno, G., Rodrigo-Gámiz, M., García-Alix, A.,
1044   Jiménez-Espejo, F. J., Martínez-Ruiz, F., Anderson, R. S., Camuera, J., and
1045   Ramos-Román, M. J.: Vegetation and geochemical responses to Holocene rapid
1046   climate change in the Sierra Nevada (southeastern Iberia): the Laguna Hondera
1047   record, Clim. Past, 14, 1687-1706, 2018.

1048   Morales-Baquero, R., Pulido-Villena, E., and Reche, I.: Atmospheric inputs of
1049   phosphorus and nitrogen to the southwest Mediterranean region: Biogeochemical
1050   responses of high mountain lakes, Limnology and Oceanography 51, 830–837,
1051   2006.

1052   Moreno, A., Pérez, A., Frigola, J., Nieto-Moreno, V., Rodrigo-Gámiz, M., Martrat, B.,
1053   González-Sampériz, P., Morellón, M., Martín-Puertas, C., Corella, J. P.,
1054   Belmonte, Á., Sancho, C., Cacho, I., Herrera, G., Canals, M., Grimalt, J. O.,
1055   Jiménez-Espejo, F., Martínez-Ruiz, F., Vegas-Vilarrúbia, T., and Valero-Garcés,
1056   B. L.: The Medieval Climate Anomaly in the Iberian Peninsula reconstructed
1057   from marine and lake records, Quaternary Science Reviews, 43, 16-32, 2012.

1058   Mulitza, S., Heslop, D., Pittauerova, D., Fischer, H. W., Meyer, I., Stuut, J.-B., Zabel,
1059   M., Mollenhauer, G., Collins, J. A., Kuhnert, H., and Schulz, M.: Increase in
1060   African dust flux at the onset of commercial agriculture in the Sahel region,
1061   Nature, 466, 226-228, 2010.

1062   Munguira, M. L. and Martin, J.: The Sierra Nevada blue, Polyommatus golgus
1063   (Hiibner). In: Conservation Biology of Lycaenidae (Butterflies), New, T. R. (Ed.),
1064   IUCN, Gland, Switzerland, 1993.

1065   Nieto-Moreno, V., Martínez-Ruiz, F., Willmott, V., García-Orellana, J., Masqué, P., and
1066   Sinninghe Damsté, J. S.: Climate conditions in the westernmost Mediterranean
1067   over the last two millennia: An integrated biomarker approach, Organic
1068   Geochemistry, 55, 1-10, 2013.

1069   O'Reilly, C. H., Woollings, T., and Zanna, L.: The Dynamical Influence of the Atlantic
1070   Multidecadal Oscillation on Continental Climate, Journal of Climate, 30, 7213-
1071   7230, 2017.

1072   Observatorio del cambio global de Sierra Nevada: Linaria v1.0. iEcolab – Laboratorio
1073   de Ecología Terrestre – Universidad de Granada, http://linaria.obsnev.es, 2016.

1074   Oliva, M. and Gomez-Ortiz, A.: Late-Holocene environmental dynamics and climate
1075   variability in a Mediterranean high mountain environment (Sierra Nevada, Spain)
1076   inferred from lake sediments and historical sources, The Holocene, 22, 915-927,
1077   2012.

1078   Oliva, M., Ruiz-Fernández, J., Barriendos, M., Benito, G., Cuadrat, J. M., Domínguez-
1079   Castro, F., García-Ruiz, J. M., Giralt, S., Gómez-Ortiz, A., Hernández, A., López-
1080   Costas, O., López-Moreno, J. I., López-Sáez, J. A., Martínez-Cortizas, A.,
1081   Moreno, A., Prohom, M., Saz, M. A., Serrano, E., Tejedor, E., Trigo, R., Valero-
1082   Garcés, B., and Vicente-Serrano, S. M.: The Little Ice Age in Iberian mountains,
1083   Earth-Science Reviews, 177, 175-208, 2018.

1084   Painter, T. H., Flanner, M. G., Kaser, G., Marzeion, B., VanCuren, R. A., and Abdalati,
1085   W.: End of the Little Ice Age in the Alps forced by industrial black carbon,
1086   Proceedings of the National Academy of Sciences, 110, 15216-15221, 2013.

1087   Pauli, H., Gottfried, M., Dullinger, S., Abdaladze, O., Akhalkatsi, M., Alonso, J. L. B.,
1088   Coldea, G., Dick, J., Erschbamer, B., Calzado, R. F., Ghosn, D., Holten, J. I.,
1089   Kanka, R., Kazakis, G., Kollár, J., Larsson, P., Moiseev, P., Moiseev, D., Molau,
1090   U., Mesa, J. M., Nagy, L., Pelino, G., Puşcaş, M., Rossi, G., Stanisci, A.,
1091   Syverhuset, A. O., Theurillat, J.-P., Tomaselli, M., Unterluggauer, P., Villar, L.,
1092   Vittoz, P., and Grabherr, G.: Recent Plant Diversity Changes on Europe's
1093   Mountain Summits, Science, 336, 353-355, 2012.

1094   Pérez-Luque, A., Pérez-Pérez, R., Aspizua, R., Muñoz, J., and Bonet, F.: Climate in
1095   Sierra Nevada: present and future. . In: Change impacts in Sierra Nevada:
1096   challenges for conservation, Zamora, R., Pérez-Luque, A., Bonet, F., Barea-
1097   Azcón, J., and Aspizua, R. (Eds.), Consejería de Medio Ambiente y Ordenación
1098   del Territorio, Junta de Andalucía, Andalucia, 2016.

1099   Pulido-Villena, E., Reche, I., and Morales-Baquero, R.: Food web reliance on
1100   allochthonous carbon in two high mountain lakes with contrasting catchments: a
1101   stable isotope approach, Canadian Journal of Fisheries and Aquatic Sciences, 62,
1102   2640–2648 2005.

1103   Ramos-Román, M. J., Jiménez-Moreno, G., R.S., A., García-Alix, A., Toney, J. L.,
1104   Jiménez-Espejo, F. J., and Carrión, J. S.: Centennial-scale vegetation and North

Atlantic Oscillation changes during the Late Holocene in the southern Iberia, Quaternary Science Reviews, 143, 84-95, 2016.

Rampen, S. W., Datema, M., Rodrigo-Gámiz, M., Schouten, S., Reichart, G.-J., and Sinninghe Damsté, J. S.: Sources and proxy potential of long chain alkyl diols in lacustrine environments, Geochimica et Cosmochimica Acta, 144, 59-71, 2014a.

Rampen, S. W., Schouten, S., Koning, E., Brummer, G.-J. A., and Sinninghe Damsté, J. S.: A 90 kyr upwelling record from the northwestern Indian Ocean using a novel long-chain diol index, Earth and Planetary Science Letters, 276, 207-213, 2008.

Rampen, S. W., Willmott, V., Kim, J.-H., Rodrigo-Gámiz, M., Uliana, E., Mollenhauer, G., Schefuß, E., Sinninghe Damsté, J. S., and Schouten, S.: Evaluation of long chain 1,14-alkyl diols in marine sediments as indicators for upwelling and temperature, Organic Geochemistry, 76, 39-47, 2014b.

Rampen, S. W., Willmott, V., Kim, J.-H., Uliana, E., Mollenhauer, G., Schefuß, E., Sinninghe Damsté, J. S., and Schouten, S.: Long chain 1,13- and 1,15-diols as a potential proxy for palaeotemperature reconstruction, Geochimica et Cosmochimica Acta, 84, 204-216, 2012.

Reche, I., Ortega-Retuerta, E., Romera, O., Pulido-Villena, E., Morales-Baquero, R., and Casamayor, E. O.: Effect of Saharan dust inputs on bacterial activity and community composition in Mediterranean lakes and reservoirs, Limnol. Oceanogr, 54, 869–879, 2009.

Reimer, P. J., Bard, E., Bayliss, A., Beck, J. W., Blackwell, P. G., Ramsey, C. B., Buck, C. E., Cheng, H., Edwards, R. L., Friedrich, M., Grootes, P. M., Guilderson, T. P., Haflidason, H., Hajdas, I., Hatté, C., Heaton, T. J., Hoffmann, D. L., Hogg, A. G., Hughen, K. A., Kaiser, K. F., Kromer, B., Manning, S. W., Niu, M., Reimer, R. W., Richards, D. A., Scott, E. M., Southon, J. R., Staff, R. A., Turney, C. S. M., and van der Plicht, J.: IntCal13 and Marine13 Radiocarbon Age Calibration Curves 0–50,000 Years cal BP, Radiocarbon, 55, 1869-1887, 2013.

Rodrigo, F. S., Esteban-Parra, M. J., Pozo-Vázquez, D., and Castro-Díez, Y.: A 500-year precipitation record in Southern Spain, International Journal of Climatology, 19, 1233-1253, 1999.

Rodrigo-Gámiz, M., Martínez-Ruiz, F., Rampen, S. W., Schouten, S., and Sinninghe Damsté, J. S.: Sea surface temperature variations in the western Mediterranean Sea over the last 20 kyr: A dual-organic proxy (UK′37 and LDI) approach, Paleoceanography, 29, 87-98, 2014.

Rodrigo-Gámiz, M., Rampen, S. W., de Haas, H., Baas, M., Schouten, S., and
      Sinninghe Damsté, J. S.: Constraints on the applicability of the organic
      temperature proxies UK'37, TEX86 and LDI in the subpolar region around
      Iceland, Biogeosciences, 12, 6573-6590, 2015.

Romero-Viana, L., Kienel, U., and Sachse, D.: Lipid biomarker signatures in a
      hypersaline lake on Isabel Island (Eastern Pacific) as a proxy for past rainfall
      anomaly (1942–2006AD), Palaeogeography, Palaeoclimatology, Palaeoecology,
      350-352, 49-61, 2012.

Sánchez-Castillo, P. M.: Algas de las lagunas de alta montaña de Sierra Nevada
      (Granada, España), Acta Botánica Malacitana, 13, 21 -52, 1988.

Sánchez-López, G., Hernández, A., Pla-Rabes, S., Trigo, R. M., Toro, M., Granados, I.,
      Sáez, A., Masqué, P., Pueyo, J. J., Rubio-Inglés, M. J., and Giralt, S.: Climate
      reconstruction for the last two millennia in central Iberia: The role of East Atlantic
      (EA), North Atlantic Oscillation (NAO) and their interplay over the Iberian
      Peninsula, Quaternary Science Reviews, 149, 135-150, 2016.

Schmidt, G. A., Jungclaus, J. H., Ammann, C. M., Bard, E., Braconnot, P., Crowley, T.
      J., Delaygue, G., Joos, F., Krivova, N. A., Muscheler, R., Otto-Bliesner, B. L.,
      Pongratz, J., Shindell, D. T., Solanki, S. K., Steinhilber, F., and Vieira, L. E. A.:
      Climate forcing reconstructions for use in PMIP simulations of the last
      millennium (v1.0), Geosci. Model Dev., 4, 33-45, 2011.

Schröter, D., Cramer, W., Leemans, R., Prentice, I. C., Araújo, M. B., Arnell, N. W.,
      Bondeau, A., Bugmann, H., Carter, T. R., Gracia, C. A., de la Vega-Leinert, A.
      C., Erhard, M., Ewert, F., Glendining, M., House, J. I., Kankaanpää, S., Klein, R.
      J. T., Lavorel, S., Lindner, M., Metzger, M. J., Meyer, J., Mitchell, T. D.,
      Reginster, I., Rounsevell, M., Sabaté, S., Sitch, S., Smith, B., Smith, J., Smith, P.,
      Sykes, M. T., Thonicke, K., Thuiller, W., Tuck, G., Zaehle, S., and Zierl, B.:
      Ecosystem Service Supply and Vulnerability to Global Change in Europe,
      Science, 310, 1333-1337, 2005.

Shimokawara, M., Nishimura, M., Matsuda, T., Akiyama, N., and Kawai, T.: Bound
      forms, compositional features, major sources and diagenesis of long chain, alkyl
      mid-chain diols in Lake Baikal sediments over the past 28,000 years, Organic
      Geochemistry, 41, 753-766, 2010.

Sicre, M.-A., Jalali, B., Martrat, B., Schmidt, S., Bassetti, M.-A., and Kallel, N.: Sea
      surface temperature variability in the North Western Mediterranean Sea (Gulf of

1173   Lion) during the Common Era, Earth and Planetary Science Letters, 456, 124-133,

1174   2016.

1175   Sigl, M., Winstrup, M., McConnell, J. R., Welten, K. C., Plunkett, G., Ludlow, F.,

1176   Buntgen, U., Caffee, M., Chellman, N., Dahl-Jensen, D., Fischer, H., Kipfstuhl,

1177   S., Kostick, C., Maselli, O. J., Mekhaldi, F., Mulvaney, R., Muscheler, R.,

1178   Pasteris, D. R., Pilcher, J. R., Salzer, M., Schupbach, S., Steffensen, J. P., Vinther,

1179   B. M., and Woodruff, T. E.: Timing and climate forcing of volcanic eruptions for

1180   the past 2,500 years, Nature, 523, 543-549, 2015.

1181   Sinninghe Damsté, J. S., Rampen, S., Irene, W., Rijpstra, C., Abbas, B., Muyzer, G.,

1182   and Schouten, S.: A diatomaceous origin for long-chain diols and mid-chain

1183   hydroxy methyl alkanoates widely occurring in quaternary marine sediments:

1184   indicators for high-nutrient conditions, Geochimica et Cosmochimica Acta, 67,

1185   1339-1348, 2003.

1186   Smith, M., De Deckker, P., Rogers, J., Brocks, J., Hope, J., Schmidt, S., Lopes dos

1187   Santos, R., and Schouten, S.: Comparison of U37K′, TEX86H and LDI

1188   temperature proxies for reconstruction of south-east Australian ocean

1189   temperatures, Organic Geochemistry, 64, 94-104, 2013.

1190   Spanish National Weather Agency - AEMet Open Data: AEMet Open Data.

1191   http://www.aemet.es/es/datos_abiertos/AEMET_OpenData, 2019.

1192   Steinhilber, F., Beer, J., and Fröhlich, C.: Total solar irradiance during the Holocene,

1193   Geophysical Research Letters, 36, 2009.

1194   Stuiver, M. and Quay, P. D.: Changes in Atmospheric Carbon-14 Attributed to a

1195   Variable Sun, Science, 207, 11-19, 1980.

1196   Tejedor, E., Saz, M. Á., Cuadrat, J. M., Esper, J., and de Luis, M.: Temperature

1197   variability in the Iberian Range since 1602 inferred from tree-ring records, Clim.

1198   Past, 13, 93-105, 2017.

1199   Theroux, S., D'Andrea, W. J., Toney, J., Amaral-Zettler, L., and Huang, Y.:

1200   Phylogenetic diversity and evolutionary relatedness of alkenone-producing

1201   haptophyte algae in lakes: Implications for continental paleotemperature

1202   reconstructions, Earth and Planetary Science Letters, 300, 311-320, 2010.

1203   Titos Martínez, M.: Los trabajos de desagüe de las lagunas de Sierra Nevada: un largo

1204   despropósito medioambiental, Revista del Centro de Estudios Históricos de

1205   Granada y su Reino, 2019. 223-243, 2019.

1206   Titos Martínez, M. and Ramos Lafuente, A. J.: El refugio más antiguo de Sierra
1207   Nevada: Construido en 1891, aún se mantiene en pie, Andalucía en la historia,
1208   2016. 48-53, 2016.

1209   Trouet, V., Esper, J., Graham, N. E., Baker, A., Scourse, J. D., and Frank, D. C.:
1210   Persistent Positive North Atlantic Oscillation Mode Dominated the Medieval
1211   Climate Anomaly, Science, 324, 78-80, 2009.

1212   Versteegh, G. J. M., Bosch, H. J., and De Leeuw, J. W.: Potential palaeoenvironmental
1213   information of C24 to C36 mid-chain diols, keto-ols and mid-chain hydroxy fatty
1214   acids; a critical review, Organic Geochemistry, 27, 1-13, 1997.

1215   Villanueva, L., Besseling, M., Rodrigo-Gámiz, M., Rampen, S. W., Verschuren, D., and
1216   Sinninghe Damsté, J. S.: Potential biological sources of long chain alkyl diols in a
1217   lacustrine system, Organic Geochemistry, 68, 27-30, 2014.

1218   Volkman, J. K., Barrett, S. M., and Blackburn, S. I.: Eustigmatophyte microalgae are
1219   potential sources of C29 sterols, C22–C28 n-alcohols and C28–C32 n-alkyl diols
1220   in freshwater environments, Organic Geochemistry, 30, 307-318, 1999.

1221   Waters, C. N., Zalasiewicz, J., Summerhayes, C., Barnosky, A. D., Poirier, C.,
1222   Gałuszka, A., Cearreta, A., Edgeworth, M., Ellis, E. C., Ellis, M., Jeandel, C.,
1223   Leinfelder, R., McNeill, J. R., Richter, D. d., Steffen, W., Syvitski, J., Vidas, D.,
1224   Wagreich, M., Williams, M., Zhisheng, A., Grinevald, J., Odada, E., Oreskes, N.,
1225   and Wolfe, A. P.: The Anthropocene is functionally and stratigraphically distinct
1226   from the Holocene, Science, 351, 2016.

1227   Willmott, V., Rampen, S. W., Domack, E., Canals, M., Sinninghe Damsté, J. S., and
1228   Schouten, S.: Holocene changes in Proboscia diatom productivity in shelf waters
1229   of the north-western Antarctic Peninsula, Antarctic Science, 22, 3-10, 2010.

1230   Yu, M., Zhang, H., Li, L., and Zhao, M.: Spatial Distributions and Potential Sources of
1231   Long Chain (C30, C32 1,15-) Alkyl Diols in Surface Sediments from Eastern
1232   China Marginal Seas, Journal of Ocean University of China, 17, 1114-1122, 2018.

1233

1234 **FIGURES**
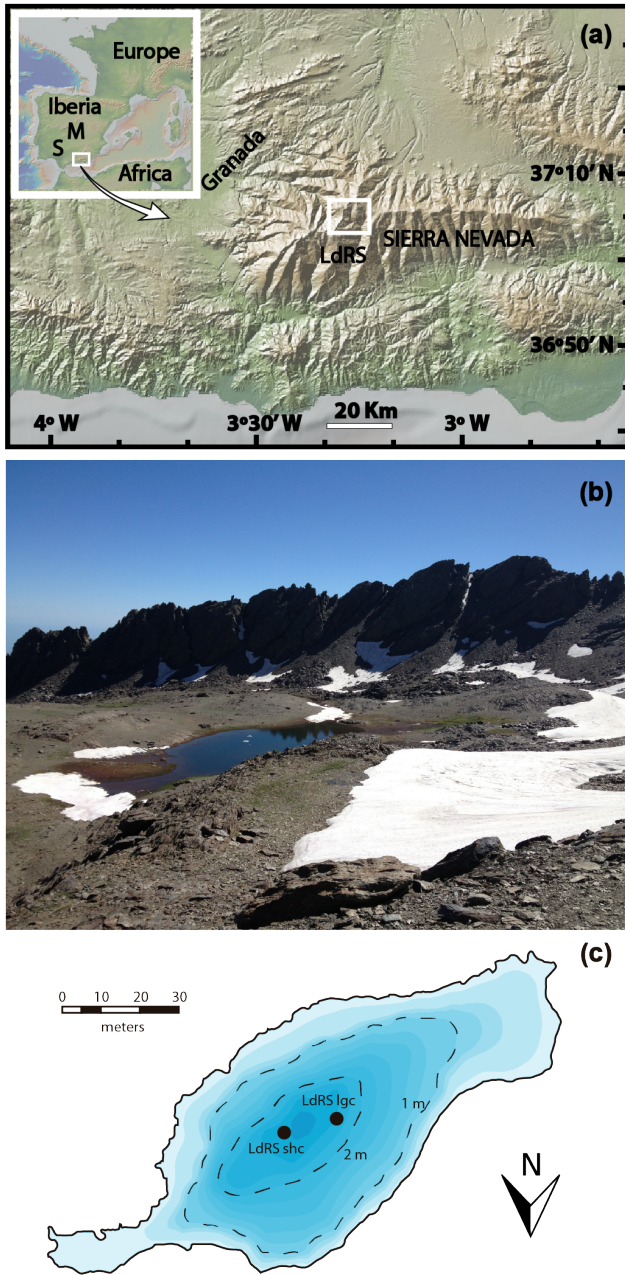
1235

1236 **Figure 1. Geographical setting. (a**) Location of the Sierra Nevada in the western

1237 Mediterranean region, Madrid (M), Sevilla (S) and Granada observatories, as well as the

1238 studied area: Laguna de Río Seco (LdRS), (**b**) LdRS catchment basin (0.42 ha) in spring

1239 2013, (**c**) bathymetry map of LdRS along with the sampling points of both cores. Data

1240 source and software: (**a**) map created by A. García-Alix using GeoMapApp (3.6.6)

1241 (http://www.geomapapp.org), (**b**) picture from A. García-Alix, (**c**) digitalized map of a

1242 bathymetry report from Egmasa S.A.
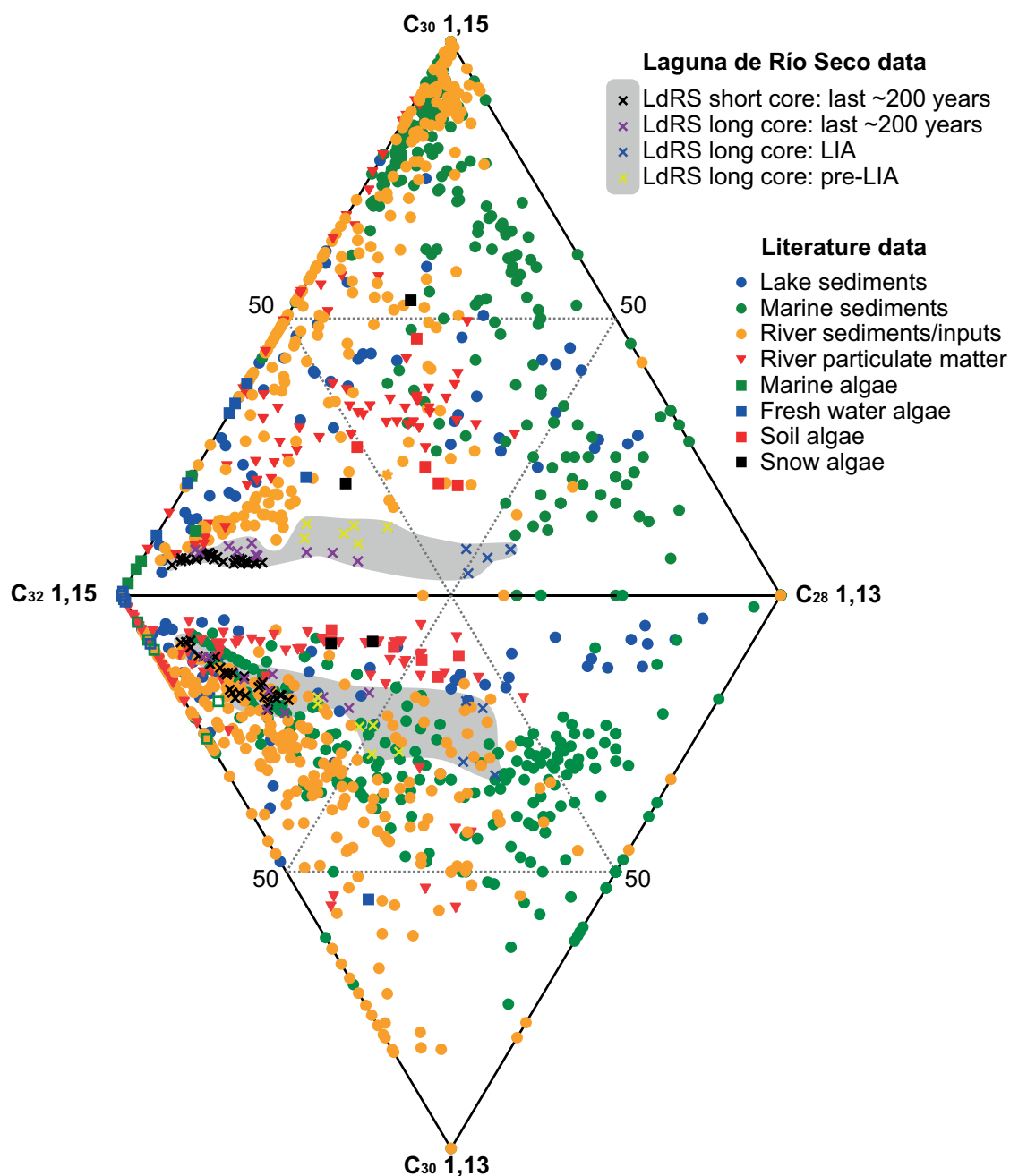
1243

Figure 2. Double-ternary diagram of the relative abundances of the C_{28} 1,13-diol, C_{30}
1,13-diol, C_{30} 1,15-diol, and C_{32} 1,15-diol from LdRS short core (LdRS shc ~200 years)
and LdRS long core (LdRS lgc ~1500 years). Diol data compiled from the literature: lake
sediments (Rampen et al., 2014a), algal cultures (Rampen et al., 2014a), marine sediments
(de Bar et al., 2016; Lattaud et al., 2017a; Rampen et al., 2014b; Rampen et al., 2012),
river sediments/inputs (de Bar et al., 2016; Lattaud et al., 2017b), river particulate organic
matter (Lattaud et al., 2018a).
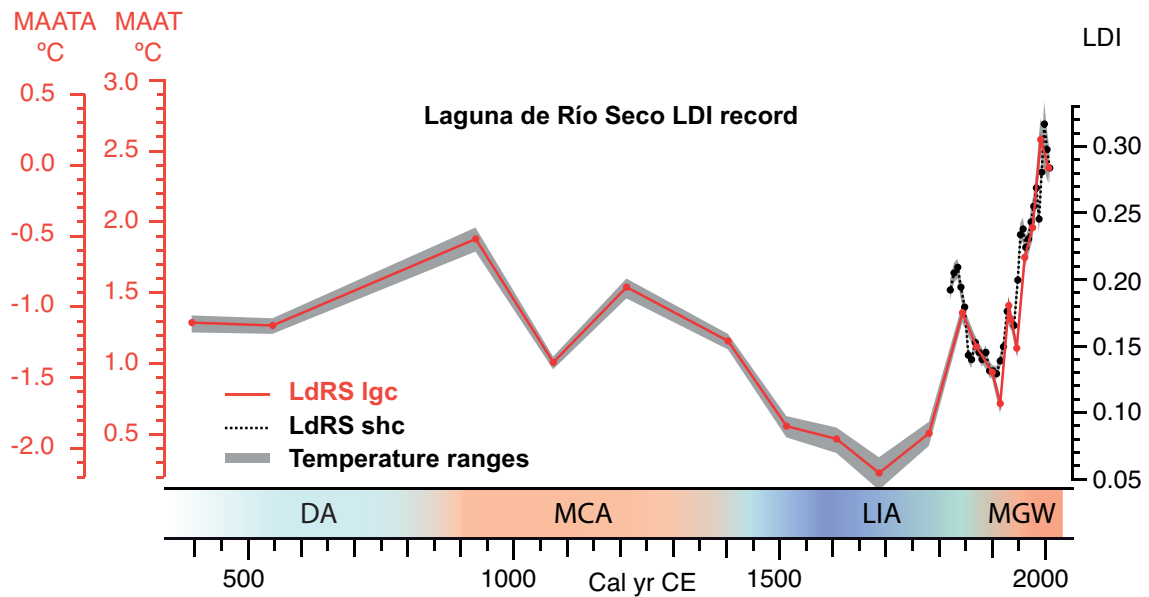
1251

1252 **Figure 3**. LDI record from LdRS, including both long core (solid line) and short core

1253 (dashed line), mean annual air temperature (MAAT ºC) reconstruction from LDI records

1254 of LdRS, as well as mean annual air temperature anomaly reconstruction (MAATAºC)

1255 respect to the annual MAAT of the last 30 years (1979-2008). The grey shade shows the

1256 reconstructed maximum and minimum temperature ranges obtained from the four LDI

1257 individual calibrations.
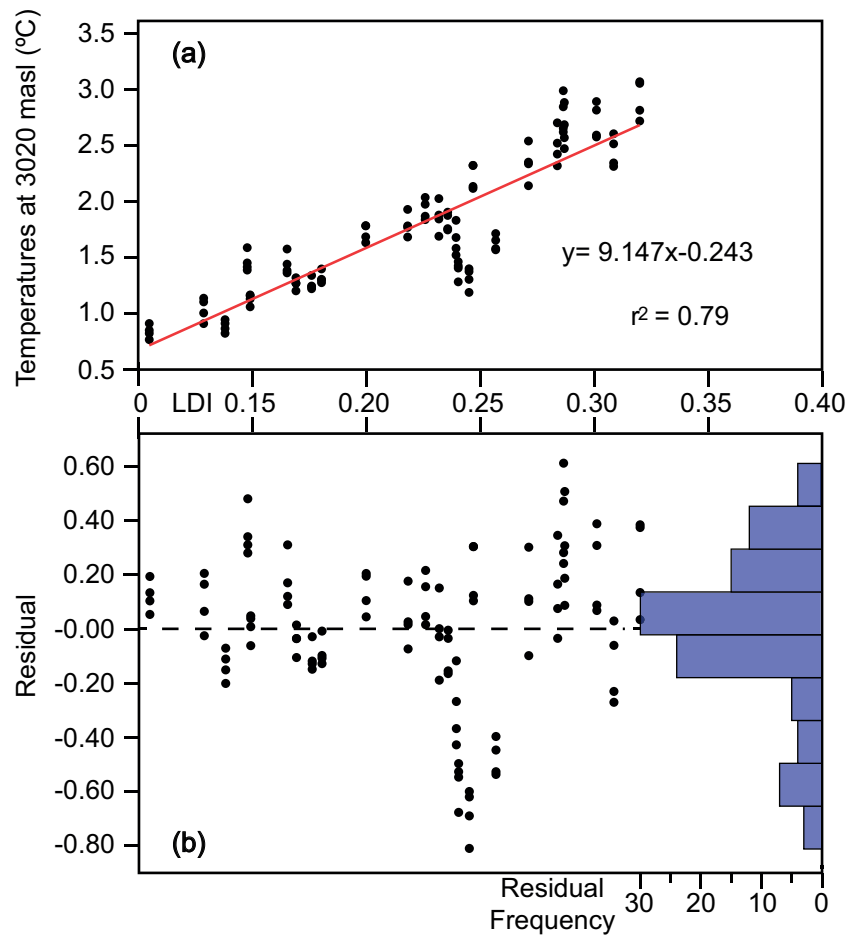
1258

1259

Figure 4. LDI temperature calibration. **(a)** Correlation by means of ordinary least square regression between both LDI records from LdRS (from 1908 to 2008) and the four reference temperature time-series at 3020 masl. **(b)** LDI values of LdRS *vs* residual temperatures (calculated between the calibrated LDI temperatures *vs* reference temperature time series at 3020 masl), as well as the histogram of the frequency of these residuals.
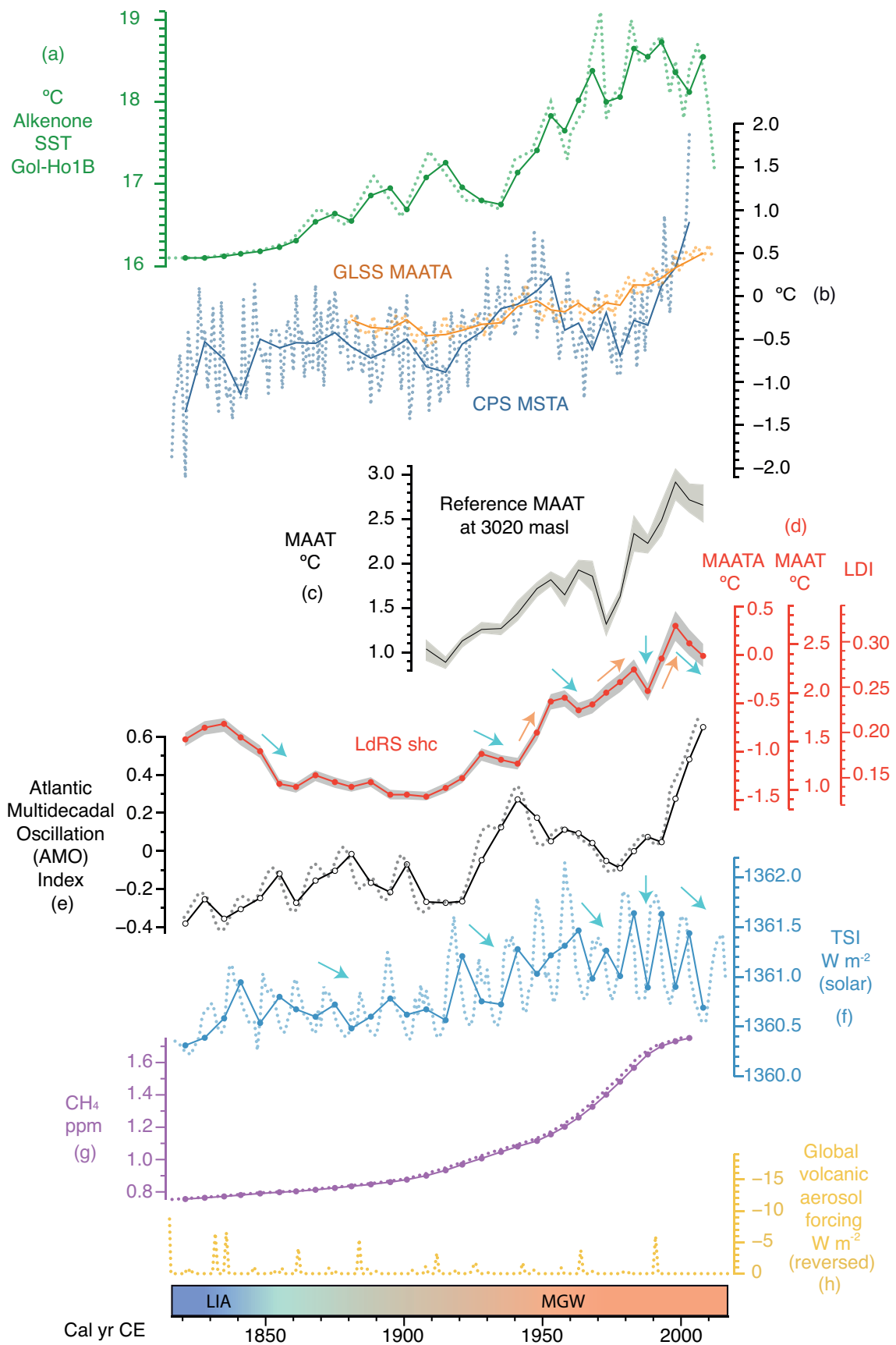
1266

1267 **Figure 5. Comparison of the LDI record and the reconstructed temperatures for the**

1268 **last ~200 years of LdRS with marine and terrestrial temperature records, Atlantic**

multidecadal oscillations, greenhouse gases, solar radiation and volcanic eruption records. Original data are in dashed lines. Solid lines represent the same time averaging as the LDI data in LdRS shc (data were linearly interpolated and time-averaged to the same resolution as the sampling points of LdRS shc) to facilitate the correlation. **(a)** Alkenone-derived Sea Surface Temperatures (SST, ºC) of the core Gol-Ho1B_KSGC-31 (Gulf of Lion: NW Mediterranean Sea (Sicre et al., 2016)), **(b)** Composite-plus-scaling (CPS) mean summer temperature anomaly reconstruction from tree rings records in Europe with respect to 1974-2003 (MSTA ºC) (Luterbacher et al., 2016) as well as global land and sea surface (GLSS) mean annual temperature anomalies with respect to 1979-2008 CE (MAATA ºC) (Hansen et al., 2010), (c) Summary of the four reference temperature time-series at 3020 masl: grey shade shows the maximum and minimum temperature range and the black solid line represent the mean temperature values, **(d)** LDI record along with the reconstructed mean annual air temperatures (MAAT ºC) and mean annual air temperature anomalies with respect to 1979-2008 CE (MAATA ºC) for the last ~200 years in LdRS, **(e)** Atlantic Multidecadal Oscillation (AMO) reconstruction (Mann et al., 2009), **(f)** high-resolution total solar irradiance reconstruction (TSI, W m^{-2}) (Coddington et al., 2016), **(g)** reconstructed concentration of atmospheric CH_4 (ppm) (Schmidt et al., 2011), and **(h)** reconstruction of the global volcanic aerosol forcing (W m^{-2}) (reversed) (Sigl et al., 2015). Acronyms: LIA, Little Ice Age; MGW, Modern Global Warming. Blue arrows: decrease; orange arrows: increase.
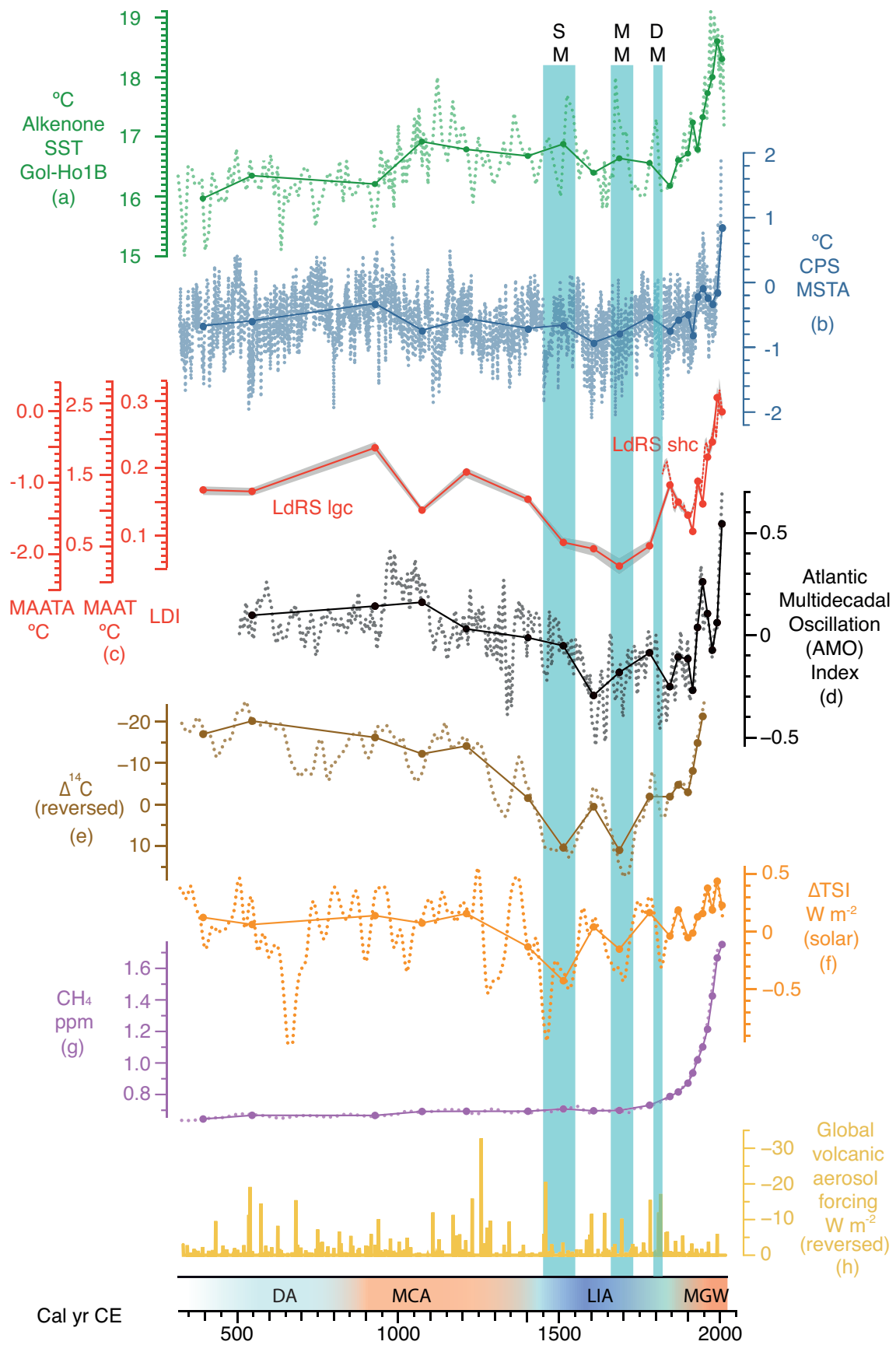
1289

Figure 6. Comparison of the LDI record and the reconstructed temperatures for the

last ~1500 years of LdRS with marine and terrestrial temperature records, Atlantic

multidecadal oscillations, solar radiation, greenhouse gases, and volcanic eruption records. Original data are in dashed lines. Solid dots represent the same time averaging as the LDI data in LdRS lgc (data were linearly interpolated and time-averaged to the same resolution as the sampling points of LdRS lgc) to facilitate the Pearson correlation: **(a)** Alkenone-Sea Surface Temperatures (SST, ºC) of the core Gol-Ho1B_KSGC-31 (Gulf of Lion: NW Mediterranean Sea (Sicre et al., 2016)), **(b)** Composite-plus-scaling (CPS) mean summer temperature anomaly reconstruction from tree rings records in Europe with respect to 1974-2003 CE (MSTA ºC) (Luterbacher et al., 2016), **(c)** LDI record along with the reconstructed mean annual air temperatures (MAAT ºC) and mean annual air temperature anomalies with respect to 1979-2008 CE (MAATA ºC) for the last 1500 years in LdRS, **(d)** Atlantic Multidecadal Oscillation (AMO) reconstruction (Mann et al., 2009), **(e)** $\Delta^{14}C$ in the atmosphere (reversed) (Reimer et al., 2013), **(f)** reconstruction of the difference of the total solar irradiance from the value of the PMOD composite series during the solar cycle minimum of the year 1986 CE (1365.57 W m^{-2}) (ΔTSI) (Steinhilber et al., 2009), **(g)** reconstructed concentration of atmospheric CH_4 (ppm) (Schmidt et al., 2011), and **(h)** reconstruction of the global volcanic aerosol forcing (W m^{-2}) (reversed) (Sigl et al., 2015). Acronyms: DA, Dark Ages; MCA, Medieval Climate Anomaly; LIA, Little Ice Age; MGW, Modern Global Warming. Blue bars show three low solar activity periods, the Spörer Minimum (SM), the Maunder Minimum (MM), and the Dalton Minimum (DM).

1314
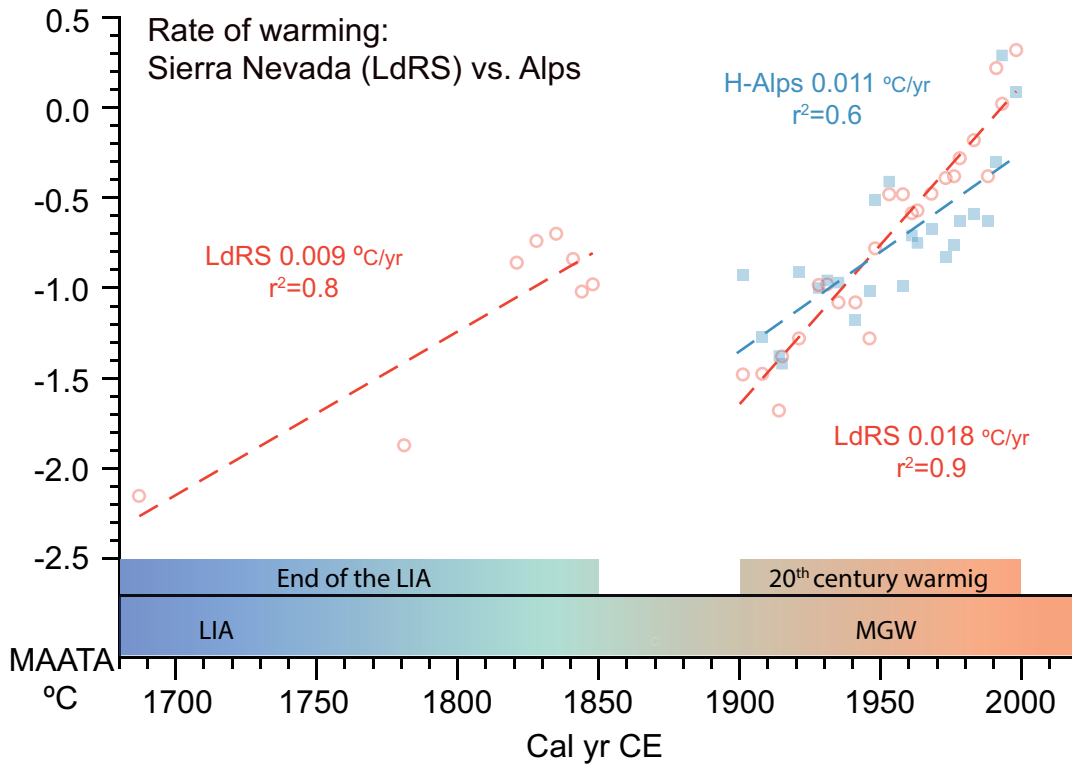
Figure 7. Comparison between the average temperature warming rates from LdRS and the alpine areas of the Alps by means of ordinary least square regressions. LDI-deduced MAATA (respect to the period 1979-2008 CE) from LdRS long and short cores for the last stage of the LIA and the 20th century (red open circles), and high-Alps historical (homogenised) temperature records from the Historical Instrumental Climatological Surface Time Series of the Greater Alpine Region (HISTALP) database (Auer et al., 2007; Böhm et al., 2010) at the same time averaging as LdRS shc-lgc to facilitate the comparison (blue closed squares).
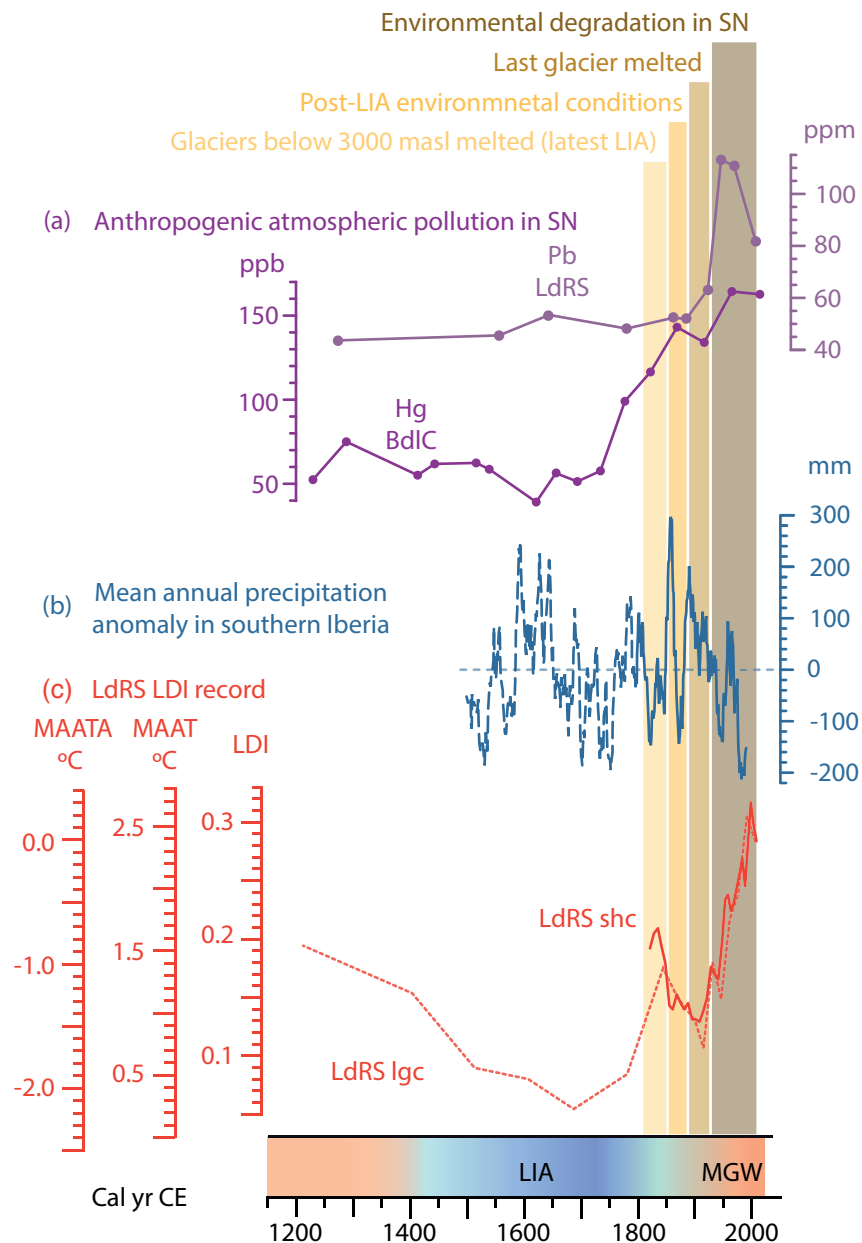
1323

Figure 8. Comparison among different factors affecting the environmental evolution of alpine wetlands in the Sierra Nevada. (a) records of anthropogenic heavy metal atmospheric pollution (Pb and Hg) in two alpine sites of the Sierra Nevada: Laguna de Río Seco (LdRS) and Borreguil de la Caldera (BdlC) (Garcia-Alix et al., 2017; Garcia-Alix et al., 2013), **(b)** mean annual precipitation anomaly in southern Iberia from 1500 to 1990 CE with respect to the mean value of the instrumental period (1791-1990 CE): solid line- instrumental data from Gibraltar (southern Iberia); dashed line- precipitation anomaly reconstruction (Rodrigo et al., 1999), **(c)** LDI and reconstructed temperatures in LdRS. Colour bars indicate the four main environmental stages in the Sierra Nevada (SN) during the last 200 years. Acronyms: LIA, Little Ice Age; MGW, Modern Global Warming.